Theoretical Aerodynamics in Today's Real World: Opportunities and Challenges

Norman D. Malmuth
Rockwell Scientific Company, Thousand Oaks, California 91360

In spite of the computational fluid dynamics revolution, significant challenges still face aerodynamicists in predicting and controlling various classes of flows. These include three-dimensional separation, boundary-layer transition, interaction of separation and transition such as on re-entry capsules, multi-element airfoils and wings, unmanned aerial vehicle low Reynolds number flows, and high angle of attack applications. Others include multi-body flows such as those occurring in store and stage separation, stiff combustion reacting and unsteady flows, as well as plasma aerodynamics and turbulence, to name a few. In many cases, diverse multiple scales are involved, and the proper identification and treatment of associated disparate length and timescales is critical in obtaining accurate prediction and effective control. The solution of such multiscale problems can be a hurdle to effective domain decomposition, even overset, unstructured adaptive gridding, and, ultimately, solution accuracy. Theoretical insights can help make proper decisions on numerical pre-processing, solution, postprocessing, and interpretation. Opportunities for a combined theoretical, computational, and experimental approach will be discussed. These will be illustrated by examples. As compared to the limited "pen and paper" theoretical methods of the 1950s, examples will be given of the effectiveness of combined asymptotics, similitude, group invariance, approximate physics-based modeling and numerical methods for conceptual vehicle design, flow control innovation, identification of key parameters, leveraging of computational solutions, reducing the parameter space, as well as providing added insight into the basic physical processes. These will be related to tradeoffs between accuracy and response speed in typical aerospace environments.

Nomenclature

A	=	admittance coefficient
AR	=	aspect ratio
$B(x, y, z)$	=	body surface
b	=	wing semispan
C_{D_w}	=	wave drag coefficient
C_P	=	pressure coefficient
c	=	wing root chord, phase speed
D_w	=	wave drag
D_{w_i}	=	wave drag first approximation
d^*	=	jet exit width
$f(x)$	=	wing shape function in constant span plane, jet shape function
$G_1(x)$	=	second term in inner expansion for perturbation potential
H	=	hypersonic similarity parameter
H_0	=	total enthalpy
h	=	jet penetration ratio
J	=	α, freestream to jet momentum flux or dynamic pressure ratio
K	=	transonic similarity parameter
L	=	characteristic length scale
$l_1(x)$	=	cumulative lift up to the station x
M_∞	=	M, freestream Mach number
$m(x)$	=	wing camber function
N	=	Newtonian similarity parameter
O	=	large order of magnitude
o	=	small order of magnitude
p	=	pressure, pressure disturbance
q	=	dynamic pressure
Re_{tr}	=	transition Reynolds number
r, θ, x	=	polar coordinates
$\tilde{r}$	=	stretched inner radius
$S_1(x)$	=	effective source strength
T	=	temperature
t	=	time

Norman D. Malmuth is a Senior Scientist and Program Manager, Fluid Dynamics, Material Sciences, Rockwell Scientific Co. He obtained his B.A.E. in aeronautics, University of Cincinnati, in 1953; M.A.E. in aeronautics, Polytechnic Institute of Brooklyn, in 1956; and Ph.D. in aeronautics at the California Institute of Technology, in 1962. Dr. Malmuth has been with the Science Center for more than 37 years and was with Rockwell International, Los Angeles Division, for 12 years and Grumman Aircraft for 3 years. Dr. Malmuth received the Distinguished Alumnus Award at the University of Cincinnati in 1990 and the AIAA Aerodynamics Award in 1991. He is past Chair of the Rockwell Fluid Dynamics Technical Panel, a member of the NASA Numerical Aerodynamic Simulator Committee, AIAA Applied Aerodynamics and Fluid Dynamics Technical Committees, the Society of Industrial and Applied Mathematics, and the American Physical Society and is listed in *Who's Who in the World*. He has been a U.S. delegate to AGARD, a Fellow of the AIAA, a member of the editorial board for the *Journal of Aircraft*, and a Visiting Scientist to Rensselaer Polytechnic Institute. He has been a consultant to Aerojet. Dr. Malmuth has 120 publications, a book chapter, and four patents. He was elected as a Fellow of the American Physical Society in 1999. For the past five years he has been a member of the Caltech faculty as a Visiting Associate in the Aeronautics and Mechanical Engineering departments of Caltech. He is a currently active commerical pilot holding instrument and multiengine ratings.

Presented as Paper 2005-5059 at the AIAA 4th Theoretical Fluid Dynamics Meeting, Toronto, ON, Canada, 6–9 June 2005; received 16 June 2005; revision received 23 October 2005; accepted for publication 31 October 2005.

U	=	freestream speed
U, V, ω	=	horizontal, vertical and pitch displacements
X, Y, Z	=	Cartesian coordinates
x, y, z	=	Cartesian coordinates (overbars imply dimensional quantities)
$z_{\mathrm{LE}}(x)$	=	leading-edge shape function
α	=	angle of attack, freestream to jet momentum flux or dynamic pressure ratio, wave number
γ	=	specific heat ratio
δ	=	characteristic flow deflection parameter, or body thickness ratio
$\varepsilon_i(\delta)$	=	gauge function
θ_j	=	jet inclination angle
θ_S	=	local shock angle
λ	=	$(\gamma-1)/(\gamma+1)$
μ	=	leading edge shape exponent
μ,τ	=	coordinate stretching factors
ρ_∞	=	freestream density
τ	=	reflection coefficient
Φ	=	velocity potential
ϕ_i	=	ith approximation to perturbation potential
ω	=	complex disturbance frequency ($\mathrm{Im}\,\omega =$ growth rate)

Subscripts

ad	=	adiabatic wall
C	=	jet cavity
j	=	jet
S	=	quantity at shock
w	=	wall
∞	=	freestream quantity

Superscript

i	=	iteration counter

I. Introduction: Technical Landscape

IN the 1970s, a revolution occurred in computing nonlinear transonic and other high-speed flows with computational algorithms and computers. From this pioneering effort, computational fluid dynamics (CFD) has been an asset and workhorse for the aerospace engineer and designer in obtaining aerodynamic characteristics of complex realistic shapes in nonlinear transonic, hypersonic regimes when the flow is essentially attached to the vehicle. Yet, despite CFD's power, challenges still exist to predict drag and other quantities such as pitching and hinge moments rapidly enough for the initial phase of aircraft development known as conceptual design. Typical CFD calculations require significant amounts of preprocessing, a large portion of which involves grid generation. Conceptual design optimization also requires the study of hundreds to thousands of airplane geometry and related parametric variations, as well as the interplay of physical intuition and compromises based on aerodynamic reasoning and systems impacts. Conflicting demands exist between quick response and preprocessing. Because the latter cannot yet be universally adapted to restructure the grid quickly for rapidly changing large parameter sets and moderate reshaping, CFD's role is emphasized in later phases of preliminary and advanced design more than the conceptual one. Alternatively, it is used to anchor a selected small subset of the conceptual (basepoint) design aerodynamic predictions using other methods.

Recent reviews, assessments, and surveys of CFD approaches currently used in industry to estimate drag as well as other forces and moments are typified by Refs. 1 and 2 and other papers. As a rapid-response alternate to CFD, empirical methods have been employed in conceptual design. One such application is the use of algebraic fairings to estimate the zero-lift transonic drag rise of fighters or near the fuel consumption pinch point of hypersonic airbreathers, a salient performance obstacle. Such fairings are of limited value because their validity is restricted to the supporting data sets, and they do not apply physical ideas in a self-consistent way based on first principles. At the other extreme, large-scale Reynolds-averaged closure Reynolds-averaged Navier–Stokes (RANS) CFD and other closures such as detached–eddy simulation (DES), with careful application and study, are capable of providing excellent, high-accuracy results for nearly attached flows over a family of shapes for which there are wind tunnel and flight tests to benchmark and even, in some cases, calibrate them. However, they provide limited design direction based on gasdynamic ideas for rapid-response, optimal aerodynamic shaping. Mathematical shaping guidance is possible from modern optimization techniques such as adjoint methods, stimulated annealing, and control theory, but is implicitly restricted to small perturbations around an initial iterate. Such methods currently require high-end workstations that, with the exception of computer-aided design platforms, are atypical in today's conceptual design environment but perhaps not in that of the future. Accordingly, the question of global optimality is a challenge to such techniques. New approaches such as continuation may be a possibility in this connection.

Other nonlinear regimes that pose challenges are high angle of attack and hypersonic flows. Although continuing outstanding success occurs in CFD modeling of attached steady flows, three-dimensional separation can be a considerable challenge. Even greater stumbling blocks are environments in which boundary-layer transition strongly interacts with separation. Examples are multielement airfoils such as those occurring on flapped and slatted wings and spoilers. Others are hypersonic elevons, scramjet inlet ramps, weapons bays, flame holders, aerooptic cavities, turbine blades, and flows over the lee side of reentry body/capsules, to mention only a few. These are a challenge to common turbulence closures, even those intended to characterize transition empirically and numerically in highly nonparallel separation bubbles, such as in trapped vortex applications and wing leading edges at high angle of attack, or in low-Reynolds-number unmanned aerial vehicles (UAV) or UCAV high-altitude, long-endurance applications.

To assess the current state of the art in the prediction and control of transitional separated flows, the author organized a NATO Specialist Meeting in Prague in October 2004 that was sponsored by six NATO nations under the Research and Technology Organization Air Vehicle Technology panel (RTO/AVT).[3] A general theme was that a unified triad of theory, computation, and experiment is needed to deal with challenges of this class of commonly occurring flows. It was clear from the papers presented that direct numerical simulation (DNS) is now emerging as a fertile opportunity for characterizing the complex physics of transitional separation. Notwithstanding Moore's law and nanotechnology, it is evident that substantial advancements in the next 5–20 years will be required in computer power and algorithms to make DNS a practical tool for the accurate prediction and control of flow over flight vehicles. Formidable obstacles exist even in DNS, such as the need to specify physically meaningful and accurate boundary conditions on the computational boundaries.

Limitations of theory and experiment are well known and were a strong motivation of the CFD revolution. Accordingly, they will not be emphasized here. What is important is that new opportunities exist to have both disciplines couple with numerical modeling to predict and control the first-order flow physics. On the experimental side, although test facilities are rapidly and sadly vanishing, new instrumentation techniques including noninvasive optical diagnostics such as planar laser-induced fluorescence (PLIF) and particle image velocimetry are attractive tools to allow us to understand flow physics in many applications.

II. Theoretical Approaches

A major drawback of theoretical tools that stimulated CFD development was the former's sinability to model the flow over complex, realistic three-dimensional practical airplane shapes as well as other bodies. At the same time, a popular misconception is that theory is strictly limited to linear flows. Counterexamples are its ability to model and give useful information regarding transonic and hypersonic flows. When aligned, asymptotics and similarity/group

invariance*[4] are powerful tools to treat situations that can be difficult to treat purely computationally.

In this paper, a few examples will be discussed that illustrate application of theory in the CFD age. These provide varying interplays of theory computation and experiment. Because of space restrictions, other potent illustrations of the triad idea will be relegated to the references. It has been the author's continuing belief that the combination of elements of the aforementioned triad can provide substantial insight not possible by any single element of the trio alone. Other benefits of a combined asymptotic[5] and numerical (CAN) approach is the identification of high gradient regions such as boundary-layer and shear-layer zones that provide insight and even requirements for the gridding and zonal decompositions. Frequently, reduced-order equations (besides Euler and other approximations) are identified with the CAN approach that, when solved numerically, give the first-order physics such as nonlinear effects. Similitude arising from theoretical considerations, for example, Reynolds number and blast wave scaling, often reduces the dimensionality of the independent variable and parameter space to describe the flowfield and economize the design of experiments or even make them possible. Some have proposed that theory can facilitate interpolation between computational solutions. For three-dimensional separation such as those determining cavity flows, theory gives guidance on expected flow topologies, for example, saddle points, higher-order nodes, and other singularities as well as vortical liftoff singularities on bodies at angles of attack. The latter play a decisive role in vortical fractals, bifurcations, and interaction of feeding sheets with large-scale vortex dynamics. These determine how lee-side separations on slender bodies evolve. In fact, understanding the role of these singularities in determining the global flow pattern can augment our grasp of three-dimensional separation and help us properly interpret CFD solutions. Another benefit of theory is that it identifies the relevant time and space scales. This is especially valuable in multiscale problems. Examples are numerically stiff singular perturbation reacting flow problems such as in combustion where diverse disparate ranges of chemical rate constants occur.

Identification of the various scales allows us to decompose naturally and cascade downwardly the problem at hand into much simpler unit subproblem building blocks that, in addition to helping to understand component physical mechanisms, can be upwardly integrated to give the solution of the original problem. This is the basis of all analysis. Classical examples of this approach are Prandtl's wing and boundary-layer theories. Others are transonic and hypersonic small disturbance approximations and Newtonian theory for slender bodies developed by Cole, as well as thin shock layer and snowplow theories by the same author.

An underlying concept in the decomposition idea is the use of parameter limits in which various speed ranges can be accurately approximated in a self-consistent way using asymptotic series or expansions that become increasingly more accurate as the limits are approached. As compared to classical Taylor and other series, these limit-process expansions frequently diverge, and there is an optimum number of terms to retain to get the best approximation to the flow for a fixed value of the relevant parameter(s). In many cases, the optimum number of terms is one! Examples of limits are freestream Mach number M_∞ tending to zero (such as the Janzen–Rayleigh, Karman–Tsien approximations discussed in Ref. 6), unity, or infinity. Freestream Reynolds number Re_∞ tending to zero (Stokes and Oseen flows) and infinity (boundary-layer theory), aspect ratio $AR \to \infty$ (lifting line theory), and characteristic flow deflection $\delta \to 0$ (small disturbance theory) are other examples. Many of the aforementioned pure Mach number limits do not lead to systematic approximations (capable of successive accuracy refinements.) Those that do are called distinguished limits (DL).[5] Frequently these are obtained by more subtle double limits involving two or possibly even more parameters. Common examples are M_∞ fixed as $\delta \to 0$ [Prandtl–Glauert theory (PGT) (see Ref. 6), linearized theory,[6] and acoustics], $K \equiv (1 - M_\infty^2)/\delta^{2/3} \equiv$ the transonic similarity parameter fixed as $\delta \to 0$ [two-dimensional transonic small disturbance theory[6–8] (TSDT)], and $H = 1/(M_\infty^2 \delta^2) \equiv$ the hypersonic similarity parameter fixed as $\delta \to 0$ [Hypersonic small disturbance theory (HSDT)[6,9]]. If $\gamma \equiv$ specific heat ratio, $\lambda \equiv (\gamma - 1)/(\gamma + 1)$, then $N \equiv H/\lambda \equiv$ the Newtonian similarity parameter fixed as $\lambda \to 0$ [Newtonian thin body theory (see Ref. 9)], $AR \to 0$, and $\delta \to 0$ (slender wing or body theory[10]). Actually, Newtonian and slender body theories are within HSDT and PGT, respectively.

Once these limits are defined, approximate limit-process series/sequence/asymptotic expansions using gauge functions to measure the size of the various terms in the series can be determined. These gauge functions depend on the small or large limiting parameter. As an example, the velocity potential Φ in TSDT for flow over symmetric zero-incidence two-dimensional airfoils has the expansion in the generic form

$$\Phi(\bar{x}, \bar{y}; M_\infty, \delta) = Ux + \varepsilon_1(\delta)\phi_1(x, y; K) + \varepsilon_2(\delta)\phi_2(x, y; K) + \cdots$$

$$x = \bar{x}/(\mu(\delta)L), \qquad y = \bar{y}/(\tau(\delta)L), \qquad K \text{ fixed as } \delta \to 0 \tag{1}$$

is valid, where $\bar{x}$ and $\bar{y}$ are coordinates aligned and normal to the freestream velocity U; L is a characteristic length scale such as the airfoil chord; the perturbation potentials ϕ_i, $i = 1, 2, 3, \ldots$, are $\mathcal{O}(1)$, that is, bounded, in the TSDT limit; and the semicolon represents parametric rather than functional dependence. Here, $\varepsilon_i(\delta)$, $\mu(\delta)$, and $\tau(\delta)$ are the gauge functions. In Ref. 7, the procedures to determine these functions, are detailed. These will not be repeated here. Suffice to say that the coordinate scaling gauge functions $\mu(\delta)$ and $\tau(\delta)$ are determined by a physical feature of the flow. For transonic flows, the wave system gets steeper for $M_\infty \to 1$, or, equivalently, the TSDT limit in Eq. (1). To keep the flow structures scaled to these waves in view in the transonic limit (such as the supersonic bubble,†[11,12] for slightly subsonic freestreams), the coordinate system is stretched by that steepened scale.[5] The latter is related to the increasing Mach angle (tending to 90 deg in the TSDT limit). A similar idea holds for boundary-layer theory where a stretching is introduced for points in the boundary layer based on the boundary-layer thickness, which scales with the Reynolds number Re_∞ (Refs. 13 and 14).‡[15] At the same time, the scaling keeps the relative position of a selected observation point to the flow features invariant in the limit. Returning to TSDT, in contrast to two-dimensional flows, axisymmetric flows and three-dimensional flows in TSDT represent singular perturbation problems of boundary-layer type rather than regular perturbation ones. (See Refs. 5, 13, and 14 for more details.§[16,17]) Namely, expansions such as Eq. (1) are not uniformly valid over the entire space of the flow considered. Accordingly, local expansions are needed for various zones in singular perturbation approximations to various flows. For slender asymmetric transonic bodies, the axis of symmetry is singular, and the asymmetric generalization of Eq. (1) [the outer expansion based on the outer limit in Eq. (1)] breaks down. Therein, a different (inner expansion) is needed that is based on an inner limit and suitable coordinate rescalings. [Changes in the gauge functions $\mu(\delta)$ and $\tau(\delta)$ are required.] This scale is related to the body transverse dimension rather the Mach wave scale. Both inner and outer expansions are mutually valid in an overlap domain. An intermediate expansion and limit is developed, and both inner and outer representations are

*For a thorough description of this methodology, see Ref. 4.

†Actually, special features such as the freezing of the flow pattern occur as the Mach number approaches unity and the bubble opens up into a bow and tail shock. This is called the stabilization law. In addition to Ref. 7, detailed analyses of the flowfield have been carried out. See, for example, Refs. 11 and 12.

‡A sophisticated and more intricate discussion and analysis regarding transonic boundary layers is given by Ryzhov.[15] It uses considerable extensions of the basic ideas introduced here, in the context of the utility of uniformly valid composite expansions regarding stability of boundary layers at transonic speeds, including the development of Görtler vortices as well as different regimes and interactions.

§Another interesting problem is the breakdown of TSDT near a blunt nose. For an excellent treatment of the singular perturbation problem and correction of TSDT near the nose, see Refs. 16 and 17.

equated in this overlap intermediate region. This matching procedure plays a pivotal role in determining the gauge functions and other unknown elements of both inner and outer expansions. The boundary conditions including far-field behaviors determine others. Often, additional terms have to be added to initial trial representations to achieve this matching. These are called switchbacks.

There are some theory appellations such as shock expansion theory[6] that are not systematic approximation schemes of the foregoing type. Although these are useful engineering methods they do not belong to the class of DL nor can they be embedded in limit process asymptotic expansions based on DL such as those in the preceding paragraph. What is important is that these approaches are not capable of systematic refinement. Frequently, ad hoc approximations are attempted based on parameters that are not really parameters, namely, those that are unknown in advance and are unfortunately based on the solution being sought.

Lagerstrom's,[13,14] Kaplun's, and Cole's[5] limit-process matched asymptotics methodology uses deductive schemes as contrasted to inductive schemes. For the former, a given asymptotic framework is set up and a deterministic drill ("turn the crank" procedure) is executed to obtain the solution. Inductive methods such as local similarity (widely used in, nevertheless, valuable engineering predictive schemes based on physical intuition and reasoning) belong to less systematic approximation methods because the bookkeeping in assessing the size of the approximations is frequently not clear. Local similarity for boundary layers subject to pressure gradients exemplifies one such inductive method. Nevertheless, many of these approaches still have our respect as responsible for remarkable innovations. Often, the inductive schemes provide the groundwork for the deductive ones.

Although previous workers such as Lax,[18] Magnus and Yoshihara,[19] and others had laid much of the groundwork, the Wright Flyer of modern nonlinear CFD was the seminal paper by Murman and Cole[20] in the author's opinion. This is an excellent example of a combination of theory and modern computational methods. Although the latter have progressed considerably since the successive line overrelaxation (SLOR) scheme used, CAN is illustrated in Ref. 20. Up to this achievement, theoretical solutions of the nonlinear transonic problem were limited to hodograph solutions such as those using hypergeometric functions. Many theoretical studies evolved for mixed unit problems for the Tricomi equation, which is a hodograph map of the transonic small disturbance Kármán–Guderley equation (see Refs. 6–8). Transonic problems that could be solved by intricate analytical pen and pencil methods include transonic wedge dividers and jets, as well as sonic flows.[6] A nonasymptotic approximate approach was the local linearization and other related integral equation methods by Spreiter.[21] With the CAN approach of Ref. 20, arbitrarily shaped symmetric thin two-dimensional airfoils could be computed to obtain a systematic approximation of the first-order physics from the asymptotically derived transonic small disturbance Kármán–Guderley (KG) equation

$$[K - (\gamma + 1)\phi_x]\phi_{xx} + \phi_{yy} = 0 \tag{2}$$

where ϕ is a perturbation potential related to terms shown in Eq. (1). A critical feature was that the realistic curved shocks formed by the envelope building process in the recompression part of the supersonic bubble could be captured as part of the numerical scheme rather than assumed ones iteratively fitted into the solution as in Spreiter's methods. Application of the latter was challenging for all but the simplest shapes. Of course, a continuing issue is capturing these as sharp discontinuities with the proper Rankine–Hugoniot jumps. Much progress has been made in this direction and it will not be cited or documented here because it is well known. Still, wave trains that interact with boundary layers and shear layers that occur in inlets, ducts, supersonic weapons bay store separation, as well as Edney IV structures[¶22] in shock interference heating can provide a challenge, even for current RANS methods and especially for nonexpert code users.

In addition to inductive and other work preceding Refs. 7 and 21, the derivation of Eq. (2) is accomplished by substituting Eq. (1) into the Euler equations and retaining like-order terms. Asymptotics were used to derive the far-field computational boundary conditions for Eq. (2), and the formulation provided a close to asymptotically consistent approximation. Of course, application of the far-field boundary conditions on a finite boundary still requires some discussion of its effect on solution accuracy. This element has received only limited theoretical analysis in spite of the preference of some to map the point at infinity into a finite boundary as a workaround. The author is not clear on how this can be done, in general, as a practical workable procedure for three dimensions with even single bodies, to say nothing of multiple bodies and boundaries. As indicated earlier, the question of how to apply asymptotic far fields on finite computational boundaries is of renewed importance in connection with DNS simulations. Current RANS approaches use Riemann conditions and nonreflecting boundaries. This interface between near- and far-field approximations and its effect on solution accuracy also arises in current sonic boom simulations that patch rather than asymptotically match ray-traced acoustics far fields with CFD mid- and near fields.

To illustrate the continuing power of theoretical methods in the CFD age in relation to the foregoing remarks, formal matched asymptotic examples combined with numerics are given in Secs. III and IV. In Secs. V and VI, nonformal asymptotic approaches blended with computational methods are described. Within the context of this paper, even the nonformal approaches are approximate physics-based models created from asymptotic ideas. In Sec. V, an engineering method is described for modeling and understanding jets in hypersonic cross flows. In Sec. VI, a new passive hypersonic laminar flow control scheme is described. The first example is provided in considerably greater mathematical detail than the others to show how the CAN approach can be applied. Space limitations relegate details of the analyses for the others to be given in the references.

III. Transonic Wave Drag Due to Lift

A. Background

An important issue in high-speed vehicle performance is transonic wave drag rise. Wing–body blending and area ruling are well-known tools that have been applied to deal with this issue. Before modern computational optimization methods, the widely publicized area ruling philosophy was mostly based on the linear supersonic area rule specialized to $M_\infty = 1$. This approach usually neglects drag due to lift as well as nonlinear effects. As indicated earlier, computational optimization usually addresses small perturbations about some baseline configuration. A more global approach is needed to account for the nonlinearities and to develop a design philosophy from first physical principles. The nonlinear area and Oswatitisch and Keune[23] equivalence rules from TSDT and nonlinear slender body theory provide valuable tools to approach these goals. As an illustration of CAN and the concepts, optimum wing planform shaping to minimize transonic wave drag due to lift will be discussed. Full details are given in Ref. 24.

Figure 1 shows a typical configuration that we have studied in connection with wing planforms that minimize transonic wave drag due to lift. This quantity can significantly affect range and other vehicle performance metrics. We consider the lift-dominated DL in which $A \equiv \alpha/\delta \to \infty$ in the TSDT body limit $\delta \to 0$. To make the approximations more transparent, two dimensionally cambered, untwisted lifting wings of zero thickness with aspect ratio of order unity were treated in this study. An inner expansion, which starts as Jones's theory, was matched to a nonlinear outer transonic theory as in excellent earlier work in Refs. 25–28.

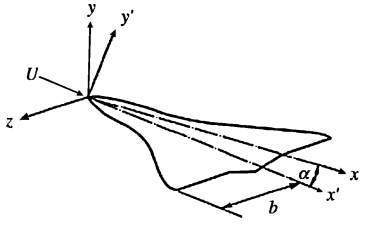

Fig. 1 Wing planform for drag rise studies.

[¶]For details, see ref. 22.

To clarify issues, to minimize ad hoc assumptions existing in earlier studies, as well as to provide a systematic expansion scheme, the aforementioned deductive approach was used with the aid of intermediate limits and matching not documented for this problem in previous literature. A new expression for the dominant approximation of the wave drag due to lift was derived. The main result is that although wave drag due to lift integral has the same form as that due to thickness, the source strength of the equivalent body depends on streamwise derivatives of the lift up to a streamwise station rather than the streamwise derivative of cross-sectional area. Some examples of numerical calculations and optimization studies for different configurations are given that provide new insight on how to carry the lift with planform shaping (as one option) so that wave drag can be minimized.

B. Theoretical Analysis

As in Eq. (1), we allow the velocity potential Φ that satisfies the full potential equation to be expanded into the asymptotic expansion,

$$\Phi(x, y, z; M_\infty, \alpha) = U\{x + \varepsilon_1(\alpha)\phi_1(x, \tilde{y}, \tilde{z}; K) + \varepsilon_2(\alpha)\phi_2(x, \tilde{y}, \tilde{z}; K) + \varepsilon_3(\alpha)\phi_3(x, \tilde{y}, \tilde{z}; K), \cdots \tag{3a}$$

in the TSDT limit

$$K = \left(1 - M_\infty^2\right)\Big/\varepsilon_1(\alpha), \qquad \tilde{y}, \tilde{z} \text{ fixed as } \varepsilon_1 \to 0 \tag{3b}$$

where K is the transonic small disturbance parameter and $\varepsilon_1(a) \to 0$ as the angle of attack $\alpha \to 0$, (x, y, z) are a nondimensionalized Cartesian frame with respect to c, the body length, and the tilded coordinates are strained in accordance with the preceding discussion, that is, $\sqrt{\varepsilon_1}(y, z) \equiv \tilde{y}, \tilde{z}$.

The steady inviscid boundary condition of flow tangency to the surface can be written

$$\nabla\Phi \cdot \nabla B = 0 \tag{4}$$

which holds on $B(x, y, z) = 0$, which defines the surface. We consider an untwisted wing of zero thickness specified by the angle of attack α and the camber function $m(x)$. (A body is added to the wing in the parametric studies to be discussed later.) The maximum chord of $c = 1$ and the maximum span $2b$ is $O(1)$. Thus,

$$B(x, y, z) = 0 = y - \alpha f(x) + O(\alpha^3), \qquad \begin{pmatrix} 0 < x < 1 \\ -z_{\mathrm{LE}} < z < z_{\mathrm{LE}} \end{pmatrix} \tag{5}$$

where $f(x) = m(x) - x$ and $m(1) = 1$. For a straight trailing edge at $y = 0$, the trailing vortex sheet lies in the plane $y = 0$, $x > 1$. The planform is specified by $\pm z_{\mathrm{LE}}(x)$, where $z_{\mathrm{LE}}(1) = b$.

When Eq. (3a) is substituted into the full potential or Euler equations and the analysis outlined in the preceding discussion is carried out, the dominant approximation for the perturbation potential is governed by the axisymmetric form of the KG transonic small disturbance equation (1). Namely,

$$\left[K - (\gamma + 1)\phi_{1_x}\right]\phi_{1_{xx}} + \phi_{1_{\tilde{r}\tilde{r}}} + (1/\tilde{r})\phi_{1_{\tilde{r}}} = 0 \tag{6}$$

where $\tilde{r}^2 \equiv \tilde{y}^2 + \tilde{z}^2$. This constitutes a deductive proof of the nonlinear transonic area rule, and, in accord with the earlier discussion, is an important reduction from three to two dimensions of the original problem. It therefore provides a drastic simplification of the gridding preprocessing problem. Matching reveals that the ε_i are subject to the following recursive relations:

$$\varepsilon_2\Big/\sqrt{\varepsilon_1} = \alpha, \qquad \varepsilon_3 = \alpha^2, \qquad \varepsilon_3 \log\left(1\Big/\sqrt{\varepsilon_1}\right) = \varepsilon_1 \tag{7}$$

In addition to far-field boundary conditions, Eq. (6) is subject to the singular boundary condition

$$\lim_{\tilde{r}\to 0} \tilde{r}\phi_{\tilde{r}} = S_1'(x) \tag{8}$$

which is a consequence of the inner expansion that is

$$\phi_1(x_1\tilde{r}) = S_1(x)\log\tilde{r} + G_1(x) + O(\tilde{r}^2\log^2\tilde{r}) \text{ as } \tilde{r} \to 0 \tag{9}$$

Part of this result is from the solution of the crossflow harmonic inner problem that drives the whole matching procedure. In contrast to a body of revolution in which the source strength $S_1(x)$ is proportional to the x rate of change of cross-sectional area, the source strength depends on the streamwise lift distribution $l_1(x)$. Namely,

$$S_1(x) = [(\gamma+1)/2]\left[l_1' l_1''\Big/(2\pi)^2\right] = [(\gamma+1)/8]\left[z_{\mathrm{LE}}^2(x)\right]'\left[z_{\mathrm{LE}}^2(x)\right]'' \tag{10}$$

where

$$l_1(x) = -\pi f'(x) z_{\mathrm{LE}}^2(x) \tag{11}$$

The main result is that the wave drag due to lift is given by

$$\tilde{D}_{w_1} = -2\pi\int_0^1 S_1(x)G_1'(x)\,\mathrm{d}x = 2\pi\int_0^1 S_1'(x)G_1(x)\,\mathrm{d}x \tag{12}$$

where $G_1(x)$ and $S_1(x)$ are given by Eqs. (9) and (10), respectively.

C. Computational Approach and Results

The solution of the TSDT boundary value problem for the axisymmetric KG equation subject to the far-field boundary conditions and the singular axis condition (8) would have been impossible to carry out in the pre-CFD age. Empowered by this reduced formulation and even dated SLOR numerics, the transonic small disturbance (TSD) boundary value problem is solved by lagging $G_1(x)$ in an iterative numerical procedure. It is updated from Eq. (9) after each SLOR sweep for the solution $\phi_1(x, \tilde{r})$ on a small cylinder $\tilde{r} = \sigma$, $\sigma \ll 1$. Namely,

$$G_1^{i+1}(x) = \phi_1^i(x) - S_1(x)\log\tilde{r} \tag{13}$$

where i signifies the old global iterate over the computational domain, $i + 1$ the new one, and $\phi_1(x) \equiv \phi_1(x, \sigma)$. Converged results with even the old SLOR method could be obtained on a typical modern personal computer in less than 1 min. Results from the executing code NLWAVE are plotted as C_{Dw} vs M_∞ for two different angles of attack in Fig. 2. Substantial drag due to lift is evident. The planform shape and the distribution of $l_1(x)$ that is typical appears in Fig. 3.

Another set of calculations incorporates a parabolic body of revolution (thickness ratio 0.057) and adds the source strength of this body to $S_1(x)$. A series of planforms with semispan $z_{\mathrm{LE}}(x)$ given by

$$z_{\mathrm{LE}}(x) = x(\mu - x^{\mu-1})/(\mu - 1)$$

and shown in Fig. 4 was considered for various μ, $M_\infty = 0.995$, and $\alpha = 0.2$ rad. The idea is to optimize the L/D figure of merit C_{Dw}/AR by a choice of planform. Here,

$$C_{Dw} = D_w\Big/\left(\rho_\infty U^2\Big/2\right)S, \qquad \mathrm{AR} = b^2/S$$

where S is the planform area and b is the semispan.

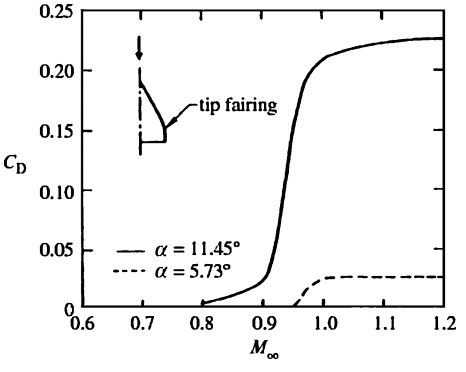

Fig. 2 Transonic wave drag rise due to lift for typical planform.

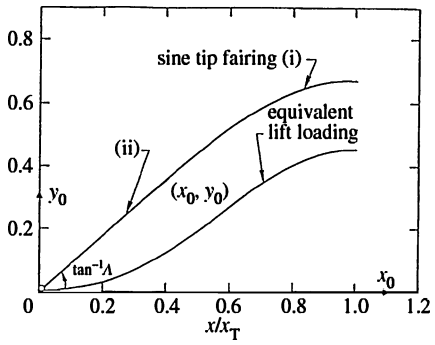

Fig. 3 Lift loading of model wing with sine tip fairing: i, $y - y_0 = [2\Lambda(x - x_0)/\pi]\sin[\pi(x - x_0)/2(x_T - x_0)]$ and ii, $y_0/x_0 = \Lambda$.

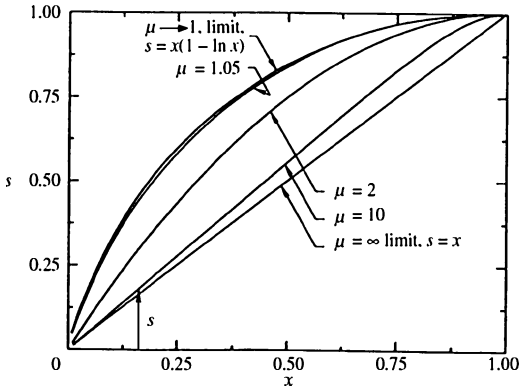

Fig. 4 Wing bodies family μ in which semispan equals $x[\mu - x^{\mu-1}/(\mu - 1)]$.

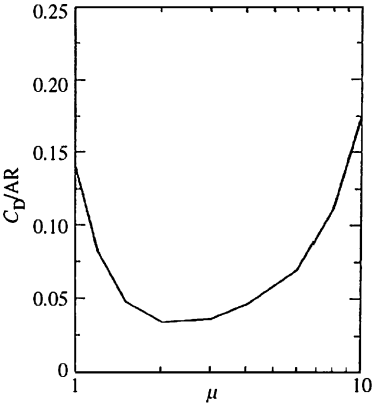

Fig. 5 Wave drag/aspect ratio figure of merit for μ wing–body family, $M_\infty = 0.9951$ and $\alpha = 0.2$ rad.

A minimum drag occurs for $\mu = 2.5$. The planform shape and curve of C_{Dw} vs μ appears in Fig. 5. Also shown in Figs. 6a–6c for $\mu = 1.2$, 2.0, and 10.0 are isobars that make evident the shock wave that occurs. As a qualitative substantiation of the minimum, the isobars and shock envelope forming process appear more intense for Figs. 6a and 6c compared to Fig. 6b. The wave drag for small μ is large because of the small sweep and for large μ because of rapid changes of $l_1(x)$ near the wing tip. These studies show the relative effectiveness of various planforms and the utility of CAN to select them in a computationally nonintense, rapid-response, desktop personal computer environment. This approach can be readily extended to study more realistic wing bodies as well as twist and thickness effects.

IV. Multibody Problems

A. Background

A challenging area for modern computational methods, theory, and experiment is the treatment of multibody problems such as store and stage separation. Typical applications are shown in Fig. 7, which shows a transonic bomb release from the B-1, weapons bay

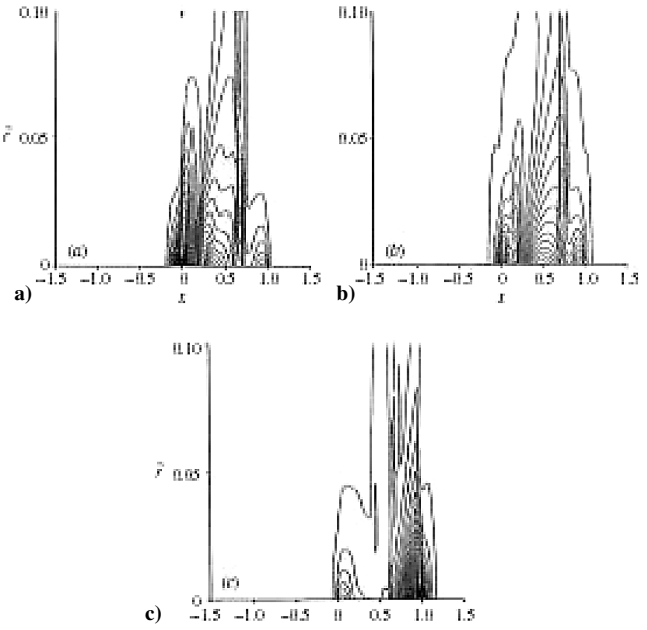

Fig. 6 Isomachs of a) $\mu = 1.2$, b) $\mu = 2.0$, and c) $\mu = 10.0$ wing–body: $M_\infty = 0.995$, $\alpha = 0.2$ rad, and $\Delta M = 0.1$.

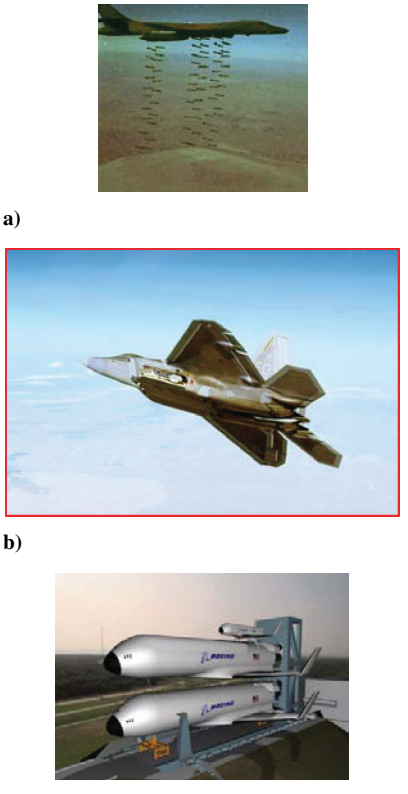

Fig. 7 Typical multibody problems: a) B-1 internal transonic store carriage and release, b) F-22 supersonic internal bay configuration, and c) hypersonic SLI stages.

arrangements on the F-22, and stage arrangements on an early space launch initiative (SLI) vehicle concept. For the latter, there is an important design trade between separation rocket motor weight and safety that is impacted by accurate prediction of stage separation aerodynamics.

Impressive progress is being made with new supercomputers and algorithms, particularly for biological flows and other applications. Major centers such as Arnold Engineering Development Center,

NASA, AFSEO, and the PET project are performing research to apply evolving techniques to store and stage separation problems. Experimentally, the captive trajectory simulation approach, in which the fluid dynamics is used as an input to a six-degree-of-freedom dynamics code to advance the body position in a two-sting wind-tunnel support system has been extensively applied to treat a class of motions where pseudosteady assumptions hold and sting interference can be accurately estimated. There are others where the validity of the pseudosteady assumptions needs to be carefully investigated. The major issue is the possibility of a difference between the time it takes for the flow to fully evolve or relax and the body motion timescale. Vortex and vorticity diffusion and convective shocks are good examples in which flow transients are disparate relative to the body motion timescales such as Froude and ejection times. Alternates to this approach are the grid method and the free drop and ejection methods with sacrificial test articles. Each of these test methods has its advantages and disadvantages. For the free drop and ejection method, a problem is the ability to relate the subscale test results to the full scale because of the lack of affordable, nontoxic (not gold, lead, or uranium) high-density materials for correct scaling of the sacrificial subscale models. Another problem is not destroying the wind-tunnel components or the cars and people in the parking lot outside of a blowdown facility. Some of this is achieved by the use of sometimes conservative light scaling rather than realistic heavy scaling in connection with the choice of Froude convective times in building the scaling parameters and the use of rigid sacrificial but not structurally tough models. An advantage is that it avoids sting interference and gives insight into unsteady effects, especially for internal weapons bay separations. In the author's opinion, a combination of all three approaches is needed as a crosscheck of any one of them. This is similar to the situation with the analytical methods.

In spite of the considerable CFD and experimental progress, major gaps exist in our ability to simulate a variety of situations. Although the trajectory of a moving body, for example, a submarine, in a fluid has received much classical attention in incompressible perfect fluid hydrodynamics, for example, Ref. 29 using apparent mass, flow kinetic energy, Hamilton's theorem, and generalized coordinates, with emphasis on coupling of the dynamics and aerodynamics, our understanding of the basic coupling physics in compressible gasdynamics, especially involving shocks, is limited, in spite of current CFD modeling capabilities.

The store separation problem has important practical applications, and its different aspects were investigated extensively using experimental and computational methods such as in Refs. 30–40. Substantial advances are being made with overset, solution-adaptive, unstructured, and moving grid approaches as indicated in these citations. Most of the studies have been concerned with *external* separation at subsonic or supersonic speeds. Relatively less attention has been given to *internal* separation from weapons bay cavities, especially at transonic speeds and the challenging supersonic and hypersonic speed ranges. A major focus at high speed is acoustic properties of the cavity. High amplitude noise arises due to feedback loops associated with stagnation of the shear layer (bounding the cavity and external flow) on the downstream cavity bulkhead. These excite structural vibrations that can cause catastrophic flight interruption from damage to the airplane. It can also destroy weapon components, including delicate guidance electronics, affecting targeting and pilot safety. This problem is very complicated due to the large number of parameters governing the flow structure and a broad variety of physical phenomena involved in the separation process. Much fundamental research has been done on empty cavities with a major focus on understanding and controlling coupling of the shear layer with the acoustic processes. Cavities filled with bodies have received only limited basic study. Computationally intense modeling RANS, DES, and even DNS to understand the acoustic excitation and the basic physics is exemplified by Refs. 41–43, among many others. A notable worthwhile exception to the empty cavity experimental emphasis is Ref. 44, which necessarily uses an invasive sting in the cavity to study the cavity shear-layer interaction in the presence of a body. Nevertheless, the results are quite illuminating, particularly when the body crosses the shear layer.

Besides the flow-induced noise and vibration problem, the cavity shear layer is an obstacle to safe separation, particularly at supersonic speeds. Our objectives are to identify first-order physical effects, simplify the key aerodynamic problems, and develop fast and reliable models for predicting store trajectories. These are intended to favorably interact with large-scale computational approaches and provide additional tools for conceptual design. An important perspective that the singular perturbation method brings to the problem is to deal with its multiscale aspects. Such a viewpoint needs to be exploited in the large-scale numerics as well. An obvious decomposition is to regard the cavity flow as a near field coupled to the global airplane midfield. Because they are over a much shorter length scale, gradients near the cavity are expected to be large compared to those over the complete airplane. In fact, the latter can be regarded as a passive scalar. We have formalized this idea with inner and outer expansions and regarded the global airplane flowfield as a weak stratification of the cavity flow that is on a much longer length scale. Both in CFD and theory, the iteration process can be envisioned in which the flow over the airplane without the cavity provides an initial iterate of boundary conditions for the local cavity inner flowfield on some computational boundary. The cavity flow is solved and then used to update the airplane flowfield. The iteration is continued until convergence. In accord with this idea and the same motivations of all of the empty cavity research, we focus on this inner problem in what follows. Understanding it is critical to studies that we are conducting with The Boeing Company on simultaneously suppressing cavity noise and achieving safe separation.[45]

Another idea that needs exploitation is that, with all of the uncertainties, prediction of the translational trajectories can be reasonably accurate in validations with experiment. A conjecture that would support this outcome is that for heavy bodies in which the aerodynamic forces are small compared to inertial or ejection ones, the flow is controlled by the latter. This is another opportunity for large-scale computational modeling in which an iteration process could be developed. Therein, the trajectory could be obtained as a sequence of iterations starting with vacuum dynamics. Small aerodynamic corrections would be introduced in subsequent iterations in which even coarse grid CFD details of the near-field cavity flow would be emphasized. Asymptotic methods may be able to provide specific elements of such an iteration process or sequence, although the execution will be dominantly computational. Here, the emphasis would not be high fidelity of the fluid dynamics, but accurate prediction of the trajectory because the fluid dynamics is only a small part of the answer for heavy bodies. Heaviness in this context needs to be specified in terms of the nondimensional ballistic parameters that compare aerodynamic forces and moments with analogous inertial quantities.

B. Summary of Theoretical Approach

Figure 8 shows the framework we used to study the near-field cavity problem. We generalized many of the ideas in the first example discussed to treat this flow. Shown in Fig. 8 is a slender body escaping from the cavity. This problem itself can be decomposed into another singular perturbation problem. Near the slender body, it is still dominated by its crossflow. Away from the body, it looks like a line source except that the latter interacts with the walls. We neglect the finite span effects and focus on the interaction of the body with the shear layer. Because the near field is crossflow dominated,

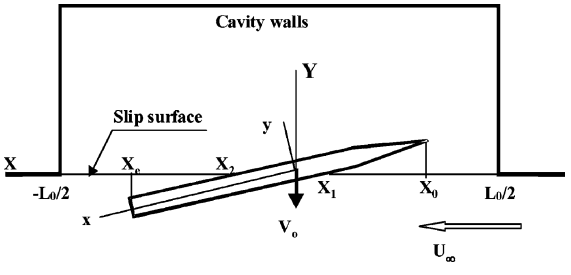

Fig. 8 Inner cavity problem.

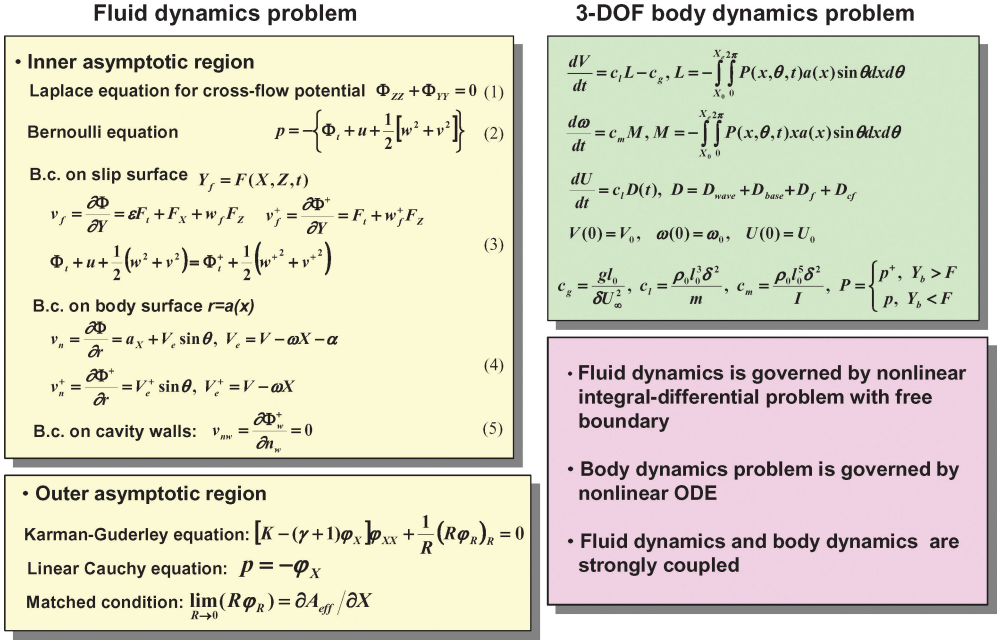

Fig. 9 Coupled dynamics and aerodynamics problem of store separation from cavity.

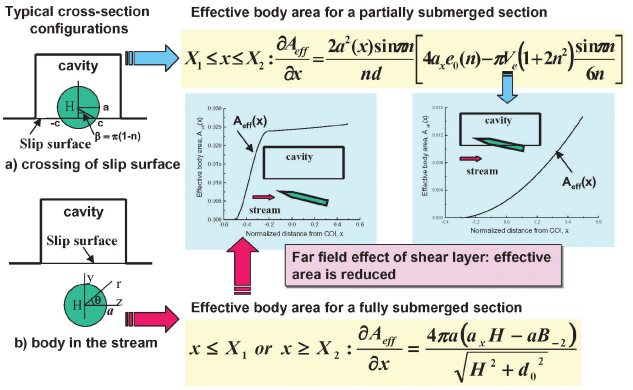

Fig. 10 Crossflow boundary-value problems for body in relation to shear layer.

various crossflow problems occur along the body. Essentially there are three cases: 1) the body is on the cavity side of the shear layer, 2) it is crossing the shear layer, and 3) it is above it the shear layer. Figure 9 shows the formulation of the problem. If (X, Y, Z) denote the normalized Cartesian wind axes, the problem obeys Laplace equation (1), in the crossflow plane (Y, Z). (Some of the equation numbers refer to those given in the designated figures rather than equations in the text of this paper.) Here, the velocity potential is denoted by $\Phi(X, Y, Z, t)$. Boundary conditions are specified on the slip surface or shear layer, $Y_f = F(X, Z, t)$. Because the flow is unsteady in the crossflow plane, the unsteady form of the Bernoulli equation (2) is used for the pressure p. This is needed because the boundary conditions are time dependent due the body motion and in spite of time not appearing explicitly in the crossflow equation of motion (1). Therefore, time is a parameter rather than an independent variable in the solution of the crossflow Laplace equation of motion. This situation is related to an assumed limit involving an unsteadiness parameter related to body motion speed in units of the flow convection speed that is characterized by a Strouhal number. In addition, the slip surface or vortex sheet boundary conditions, the tangency boundary conditions (4) and (5), respectively, on the body and cavity walls apply. Typical boundary-value problems associated with these conditions are shown in Fig. 10 for cases 2 and 3. Note that in the near field (inner flow), streamwise stations are independent of each other. In addition, it is possible to have different cross sections of the body that represent cases 1–3.

The upper right-hand panel of Fig. 9 shows the coupled set of aerodynamic and three-degree-of-freedom equations. Here, U, V, and ω, respectively, represent the horizontal, vertical, and pitch velocities; D, L, and M, respectively, represent drag, lift, and pitching moment. Initial conditions for the displacements are shown. Coupling of the aerodynamics with the dynamics is evident in these equations because D, L, and ω are computed from the pressure field as shown in the panel. For transonic freestreams, the drag D has a wave drag portion in addition to friction. The former is obtained by solving the boundary-value problem for the far-field axisymmetric KG equation shown in the bottom left hand panel in Fig. 9. This equation was discussed in the preceding example. As in the preceding example, the singular boundary condition involves the source strength $S(x) = \partial A_{\text{eff}}/\partial x$, where $A_{\text{eff}}(x)$ is the effective cross-sectional area and x is an alternate notation for X. $A_{\text{eff}}(x)$ is determined from the outer expansion for solutions of the crossflow boundary-value problems shown in Fig. 10. Determining this quantity is more involved than in the preceding example because of the more complicated near-field boundary-value problem. These solutions were worked out as generalizations of the more simple flow over a log discussed in Ref. 29. It involves the use of conformal mapping, elliptic functions, and singular integral equations in the complex plane for Riemann–Hilbert problems. The main point is that the crossing of the shear-layer physics is systematically included in the problem and that it influences the shock dynamics in the far field. Details of the analyses for subsonic, transonic, and supersonic freestreams are given in Refs. 46–48.

C. Physical Mechanisms Relative to Noise Reduction and Safe Separation of Supersonic Stores from Weapons Bay Cavities

For supersonic store separation, the formation of a bow shock over the nose of the body as it crosses the supersonic part of the shear layer is responsible for the loadings shown in Ref. 44. It can be a major reason why supersonic store ejection is so difficult as compared to subsonic ejections. The nose loading creates a nose-toward cavity pitching moment attracting the body to the cavity. This moment is unstable for the nose, namely, a pitch toward the cavity increases that tendency because the compression on the upper part of the body (that first crossed the shear layer) will be increased, and that on the lower side (that subsequently crosses the shear layer) will be decreased.

As indicated in Ref. 45 jets upstream of supersonic weapons cavities helped safe separation in tests at the Boeing Polysonic Wind Tunnel. One mechanism that enters into this method of flow control

is that a jet upstream of the cavity lip creates its own shear layer. Air-curtain-wise, the latter shields/screens the high-velocity shear-layer interface from the supersonic freestream that was there before the jet was. It produces an upwash-induced, increased angle of attack, favorable flow turning induced normal force and moment away from the cavity on the weapon. This was mimicked by a ski slope turning vane or spoiler that the author developed with The Boeing Company personnel. It counteracts the download from the shock that is present without the jet. It even might create a subsonic flow behind itself that could avoid the shock in the supersonic part of the shear layer or above it. Another possible bonus, besides the upwash that produces a normal force away from the cavity on the weapon is the fire hose effect that gives a pressure footprint on the forward part of the weapon, further forcing it away from the cavity. To determine the relative effectiveness of the fire hose effect, loads on the store from shock pressures need to be compared to loads from those from the jet momentum flux. This comparison could give appropriate nondimensional scaling parameters to size the jets and design their pneumatic supply systems. Anecdotal evidence is that although this mechanism would act for stores near the rear of the cavity, safe separation is usually obtained. It is conjectured that this might be explained by the flow toward the fins into the cavity produced by the cavity eddy circulation for deep cavities, for example, 5:1. This load could favorably compete with the unfavorable shock loads.

An additional mechanism of course comes from the jet bow shocks that can compound the favorable flow turning upwash. The jet shear layer in some sense replaces the cavity shear layer. (There will still be a small vestigial remnant of this layer as can be seen by the PLIF and schlierens by Hanson and Ben Yakar conducted at Stanford and described in more detail later in this paper.) Euler calculations with adaptive mesh refinement run by Hornung of the California Institute of Technology under collaboration with the author using James Quirk's Amrita software system described in Ref. 49 also show this behavior.

The new jet shear layer is an interface with the freestream, and its loft will avoid the noise spectra feedback loop (and its effects on the weapon) produced by stagnation of the uncontrolled shear layer on the downstream cavity bulkhead. This is because the new jet shear layer is elevated enough to reattach on the downstream horizontal surface behind and not on the cavity downstream bulkhead. This is critical in avoiding the associated feedback loop and weapon flow induced structural vibrations from shear-layer cavity downstream bulkhead stagnation. This is offset by a static stability contribution of any tail fins. In addition, the lumped parameters shown in the right upper panel of Fig. 9 collapse the test matrix and are helpful for implementing control for safe internal bay separation.

The loft of the shear layers under jet control is important in controlling the broadband and discrete fluctuations that act on the weapon when the doors open or even without doors during release. Even though the impulse time is short, fatigue can occur on an stress number of cycles s–n curve because of the amplitude of these pressure load cycles. These are transmitted to the weapon as pressure oscillations. They are probably on too short a timescale to influence the trajectory in the later stages of launch but certainly affect the electronics, fins, arming mechanisms, etc. They may also affect the initial launch conditions depending on the time of release and what is going on in the cavity at that instant.

D. Parametric Studies

Figure 11 shows some parametric studies that we have conducted with the theory just outlined. In Figs. 11 and to avoid clutter and illuminate the trajectory details in the motion sequences, only the centerline of the body is shown, in contrast to its actual cone–cylinder shape. The top two panels show incredibly marked difference between vertical initial translation V_0 imparted to the body for nearly Mach 1 freestream conditions. An approximately 30% difference in velocities makes the difference between safe escape and recontact in this example with a nose toward cavity initial pitch angle $\alpha_0 = 6$ deg. Even for transonic as a contrast to supersonic ejection, the nose-toward-cavity initial pitch provides a greater pressure on

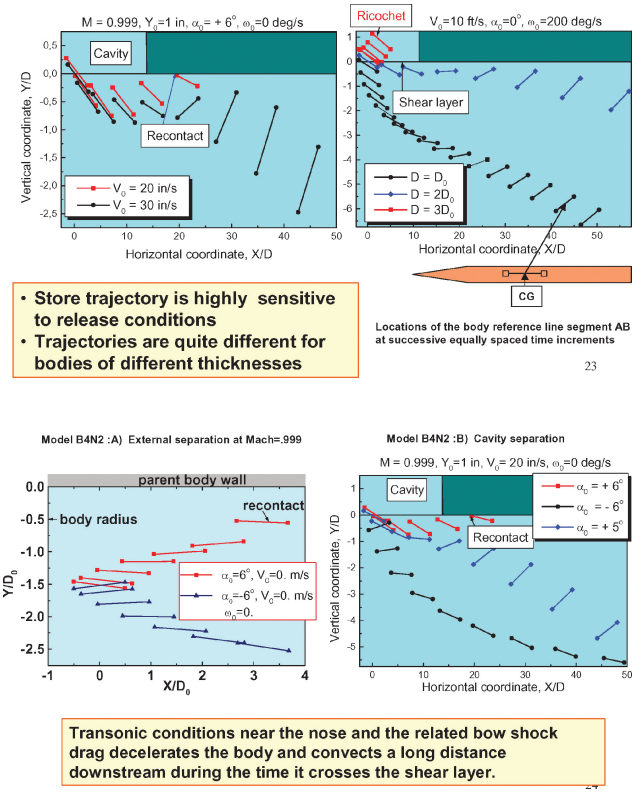

Fig. 11 Parametric studies of store escape from cavity to transonic flow.

the lower than upper side of the nose for a conical forebody, with the greater compressive flow turning tending to push the store toward the cavity. For $V_0 = 20$ fps, the pitch induced lift is not sufficiently countered by the plunge imparted to the body, whereas for $V_0 = 30$ fps there is enough plunge momentum to allow it to escape the normal suction force toward the cavity due to the fluid mechanics. As mentioned earlier, other factors that enter this equation are the phase lag between pitch and plunge as well as static stability afforded by fins.

Note that despite the missing fins, the body in this example was statically stable because it had a c.g. forward of the aerodynamic center. This is because the example parameters coincided with a body tested by Malmuth et al.[50] at the Illinois Institute of Technology low-speed tunnel for a low-speed verification of the theory in Ref. 46. The forward c.g. position was because the nose of that body was solid, and its cylindrical afterbody was hollow. Other factors that need to be further studied in this interpretation are dynamic stability and the coupling of the plunge induced unsteady flowfield, as well as the influence of the changing boundary conditions as the body is quickly projected downstream because of the significant transonic drag, which is augmented by a base drag component. In this streamwise motion, the boundary conditions change from those from the slip surface to the solid wall. The right upper panel shows a dramatic influence of body thickness ratio in which the thicker bodies tend to recontact the wall for the same release conditions as the thinner ones. This is most likely due to greater nose loading due to increased slope of the forebody with increasing thickness ratio. Evidence, however, exists that the effect of this change may damp out quite quickly above the parent body.

The bottom two panels show the effect of an initial angle of attack on store plunge and pitch trajectory. In the left upper panel, external ejection without a cavity is shown, with pitch into the surface. (Positive α_0 represents pitch to the parent body of parasite store body.) It is evident that $\alpha_0 > 0$ with zero initial pitch velocity ω_0 leads to recontact for external carriage. In contrast, $\alpha_0 < 0$ gives safe escape. The trends shown for the external release carry over the thicker body in the presence of the cavity is shown in the bottom left of Fig. 11.

V. Jets in Hypersonic Crossflows

A. Background

Performance of hypersonic airbreathing propulsion systems strongly depends on efficiencies of fuel injection and mixing in the supersonic combustion chamber. Mixing and flame stabilization may be achieved in recirculation regions and coherent structures containing unmixed fuel and air. Transverse injection, which is commonly used in the design of supersonic combustors, involves these mechanisms. This example, which is discussed in more detail in Ref. 51, shows how some of the ideas of asymptotics can be used to create a practical engineering method to estimate jet penetration in hypersonic crossflows.

These ideas and the analysis are extremely relevant to store separation from weapons bay cavities discussed in the preceding section and by use controlling it by blowing upstream of the cavity as discussed in Ref. 45. They provide actual quantitative measures for jet penetration and scaling useful for the design of jet control of weapons bay cavities and the design of relevant experiments. Although the application to store separation is in the low supersonic regime, the elasticity of Newtonian theory to lower Mach numbers than hypersonic provides a useful tool for the assessment of the jet effects on the cavity flow, specifically those related to jet penetration.

As shown in Fig. 12 (Refs. 52 and 53), the flow pattern induced by underexpanded transverse injection is rather complicated, as further indicated in Ref. 54. When the lower panel of Fig. 12 is referred to again, the fuel jet displaces the supersonic crossflow as if a bluff body were inserted into the flow. A bow shock 3, upstream of the injector exit, is formed, causing the upstream boundary layer to separate at the point S. In the separation region 1, the boundary layer and jet mix subsonically. The jet turns to the freestream direction and reattaches to the wall at the point R forming another recirculation region 6 downstream from the jet exit. This process is accompanied by formation of shocks 2 and 8 and expansion waves 7. Nevertheless, in the near-field region, the time-averaged jet-penetration profile mimics the bow shock shape and looks smooth. In the far-field region (downstream from the point A), the jet thickness continues to grow. However, this growth, which is due to the turbulent mixing rather than the pressure gradient, is much slower than that in the near-field region.

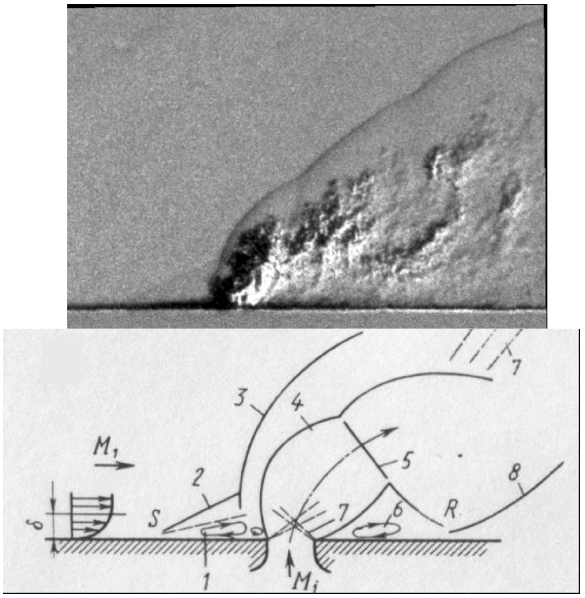

Fig. 12 Upper panel, schlieren image of normal underexpanded hydrogen injection into supersonic crossflow from Ref. 52; and lower panel, schematic of flow pattern (from Ref. 53): 1, separation bubble upstream of jet exit; 2, shock due to upstream separation at point S; 3, bow shock induced by jet; 4, jet contour; 5, Mach disk; 6, separation bubble downstream from slot; 7, expansion waves; 8, shock induced by jet reattachment R; M_1, freestream Mach number; and M_j, Mach number of outflowing jet.

The near-field mixing is driven by large-scale jet shear-layer vortices generated by the jet–freestream interaction as shown in Refs. 52 and 54. These vortices are formed along the jet–freestream interface starting near the injector exit. They periodically entrain large quantities of freestream air and draw them into the jet shear layer. In the far field, the eddies travel with velocities close to the freestream velocity. These coherent structures, where the fuel and air are mixed by slow molecular diffusion, also travel at high speeds. Consequently, the combustion process is mixing (vorticity diffusion) controlled.

Experiments discussed in Refs. 52, and 54–58 show that ignition is likely to occur in the recirculation region ahead of the jet exit. The flame is convected downstream along with the large eddies and observed near the outer edge of the jet plume. To estimate flame-holding capability of the transverse injection and stagnation pressure losses due to the jet-induced shock, it is necessary to predict the bow shock shape and the average penetration profile of the jet plume. This could be done empirically using correlations of experimental data.[53] The average penetration profile is commonly approximated by a power law fit as in Refs. 52, 53, 55, and 57 that couples the jet outer edge with the downstream distance from the jet exit. However, this correlation varies widely between experimental studies.

Although CFD approaches such as RANS and DES are nominally capable of handling jets in a crossflow, depending on turbulence modeling and use of implicit algorithms, they are time consuming in engineering practice. Quicker response, analytical models are required to shed light on the physics of jet penetration and interpolate between large-scale CFD solutions. These are also useful for conceptual and preliminary design phases associated with turnaround parametric studies. This motivated us to analyze the transverse injection into supersonic crossflow using asymptotics-related methods. We believe that such a model can shed light on previous experiments and recent large simulations. An excellent example of the latter is given in Ref. 59.

Here, the crossflow jet problem is formulated for a hypersonic freestream in the Newtonian limit[8] of the Euler equations in natural streamline coordinates.[60] Although some sort of blast wave theory[61–63] seems appropriate associated with hypersonic blunt bodies, basic ideas of the thin layer Newtonian theory[9] are also appropriate. It is shown that a shape of the thin shock-jet filament is governed by an ordinary differential equation that is solved analytically here. In addition, the analytical solution is compared with the experiments in Refs. 52, 54, and 58 on combustion and mixing of the transverse hydrogen jet injected into supersonic crossflows.

B. Basic Formulation

Consider normal injection of a fuel jet into a supersonic crossflow shown in Fig. 12. The jet displaces the supersonic flow qualitatively, as if a blunt body were inserted into the flow. In this situation, the characteristic flow deflection slope is $\delta \equiv U_j^*/U_\infty^* = O(1)$, where U_j^* is speed at the jet exit, U_∞^* is the freestream speed, and asterisks denote dimensional quantities. When it is assumed that the freestream Mach number $M \to \infty$ and the specific heat ratio $\gamma \to 1$, consider the Newtonian limit[9] of the Euler equations: $H \equiv (M\delta)^{-2} \to 0$ and $\lambda \equiv (\gamma - 1)/(\gamma + 1) \to 0$, so that $N = H/\lambda$ is fixed. Neglecting viscous shear-layer processes, we assume that U_j is constant along the jet and that the jet thickness approximately equals to the jet exit width d^*. With these assumptions, the flow pattern is shown schematically in Fig. 13. The bow shock and the outer edge of the fuel jet form a thin shock-jet filament, which is approximated by a single line $y = f(x)$ with $x = x^*/d^*$ and $y = y^*/d^*$.

Following results of the Newtonian and blunt-body theory,[9,64,65] an approximate model is based on the balance of pressure with centrifugal force inside the jet-shock filament. It is assumed that the pressure p_C^* behind the downstream boundary of the jet is of the order of the pressure in the downstream recirculation region. (See the dead-water cavity eddy 6 in Fig. 12.) This pressure is small compared to the static pressure p_S^* inside the shock-jet filament shown in Fig. 13. The latter approximately equals the pressure directly behind the shock, which is determined by the two-dimensional shock relations for a blunt-body Newtonian limit. The pressure coefficient

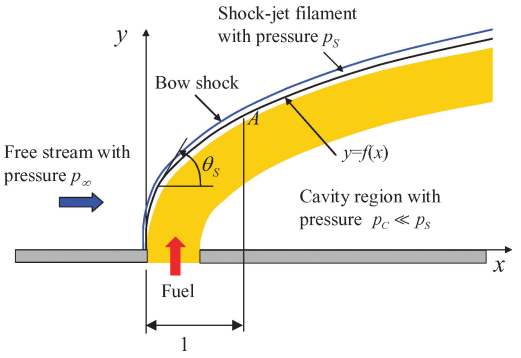

Fig. 13 Approximate flow pattern in inviscid Newtonian limit.

$C_{P_S} \equiv (p_S^* - p_\infty^*)/q_\infty^*$ is estimated as

$$C_{P_S} \cong 2\sin^2\theta_S = 2[f'^2/(1+f'^2)] \tag{14}$$

where $\tan\theta_S = f'$ specifies the local slope of the shock-jet filament (Fig. 13). This equation leads to the relation

$$p_S^* \cong 2q_\infty^*[f'^2/(1+f'^2)]$$

Along the jet-shock filament, the centrifugal force is balanced by the pressure gradient across the filament that gives[60]

$$\frac{\partial p^*}{\partial n^*} \cong \frac{\Delta p^*}{d^*} = \frac{p_S^* - p_C^*}{d^*} \cong \frac{\rho_j^* U_j^{*2}}{R^*(x)} \tag{15}$$

where n signifies the direction normal to the jet-shock filament; ρ_j is jet density, which is approximately constant along the jet length; and $d^*/R^*(x) = |f''(1+f'^2)^{-3/2}|$ is the normalized curvature of the shock-jet filament. The absolute value sign is important because for the normal injection $f'' < 0$, and imaginary limiting solutions for small x can arise if this is not taken into account.

Using the approximation $\Delta p^* \cong p_S^*$ and the equation for p_S^*, we obtain the nonlinear ordinary differential equation

$$f'^2 = \alpha\left|f''(1+f'^2)^{-\frac{1}{2}}\right| \tag{16}$$

where $\alpha \equiv q_j^*/q_\infty^*$ is the jet-to-freestream momentum flux ratio, $q_j^* = \rho_j^* U_j^{*2}/2$. The appropriate initial conditions for Eq. (16) are

$$f(0) = 0, \qquad f'(0) \to \infty \tag{17}$$

C. Solution

The problems (16) and (17) give a one-parameter family of solutions with α as the parameter. This parameter may be scaled out of Eq. (16) by the transformations

$$F(X) = f(x)/\alpha, \qquad X = x/\alpha \tag{18}$$

Substitution of Eq. (18) into Eqs. (16) and (17) gives the initial-value problem

$$F'' = -F'^2\sqrt{1+F'^2}, \qquad F(0) = 0, \qquad F'(0) = \infty \tag{19}$$

where the primes signify differentiation with respect to X. An exact solution of Eq. (19) is

$$F(X) = \log\left|(1+X) + \sqrt{(1+X)^2 - 1}\right| = \cosh^{-1}|(1+X)| \tag{20}$$

For small X relevant to the near field, the solution (20) is approximated as

$$F(X) = \log\left|1 + \sqrt{2X} + X + \cdots\right| \cong \sqrt{2X}, \qquad X \to 0 \tag{21}$$

Note that, in contrast to the blast wave theory,[61–63] the exponent in Eq. (21) should be two-thirds rather than one-half for this two-dimensional flow. This appears appropriate because the equations are not embedded in the blast wave similitude. Note that the one-half exponent applies for an axisymmetric body in the blast wave theory.

For large X, we obtain

$$F(X) \cong \log X, \qquad X \to \infty \tag{22}$$

Equation (22) shows that the shock does not become asymptotic to a Mach line, as it should. This is associated with a breakdown of thin shock layer approximations in the far-field region, where the strong shock and hypersonic approximations are inappropriate, and some form of the Prandtl–Glauert linearized theory approximations is more valid. In some form of an outer limit and asymptotic matching that has yet to be discovered, although unified supersonic–hypersonic similarity has been proposed, the body appears as a supersonic source generating a Mach wave in the far field. The yet to be determined unified theory would systematically match thin shock layer, blast wave, and linearized regions, as well as provide a uniformly valid description of the flow. Nevertheless, the physics-based engineering approximation used here provides a useful estimate for the jet penetration as will be shown in the next section.

D. Comparison with Experiment

In the empirical model of Ref. 53, the jet penetration depth h^* is defined as a distance from the point A to the wall at $x = 1$ (Fig. 13). The experimental data discussed in Ref. 52 are correlated as

$$h \equiv h^*/d^* = [1.51/(1+\cos\theta_j)]\sqrt{\alpha} \tag{23}$$

where θ_j is the jet injection angle. For the normal injection, $\theta_j = 90$ deg, the relation (23) gives $h = 1.51\sqrt{\alpha}$. Using the near-field asymptotic form (21) and validating that the point A corresponds to $x \approx 1$ as defined earlier, we obtain $h = \sqrt{(2\alpha)} \approx 1.41\sqrt{\alpha}$, which is close to the correlation (23). More importantly, the square-root singularity near the jet origin $x = 0$ predicted by the theory agrees with the empirical fit. This indicates that the analytical solution (20) resulting from the inviscid approximate thin shock layer model captures basic features of the near-field flow. As mentioned earlier, the approximation is not related to blast wave similitude and, therefore, gives a different singular behavior near the origin than that from the blast wave theory.

Ben-Yakar and Hanson[52,54] and Ben-Yakar et al.[58] performed experimental studies of combustion and mixing in high total enthalpy supersonic flows. The experiments, conducted in an expansion tube facility of Stanford University, were designed to investigate the near-field mixing and autoignition of a three-dimensional underexpanded transverse hydrogen jet injected through a cylindrical hole. Simultaneous OH–PLIF and schlieren imaging were performed at the jet centerline to obtain information on the location of shock waves, the jet penetration, and the region of combustion. These data are used hereinafter for testing our theoretical model.

In Fig. 14 the theoretical solution (20) is compared with the instantaneous schlieren images[52,58] of hydrogen and OH injection into the crossflow at $M \approx 3.5$, static temperature $T^* = 1300$ K, static pressure $p^* = 0.32$ psi, and freestream velocity $U_\infty^* = 2420$ m/s. The jet-to-freestream momentum flux ratios are $\alpha = 1.4$. Large-scale coherent vortical structures generated by the jet–stream interaction are clearly observed along the jet–freestream interface. These structures cause local fluctuations of the bow shock as documented in Ref. 51. Nevertheless, the time-averaged shock position is smooth rather than a bumpy instantaneous shape. In the near-field region $x < 3$, the jet outer edge is located close to the bow shock, forming a thin shock-jet filament that confirms our theoretical concept. In this region, the solution (20) agrees well with the average position of the jet outer edge, as shown in Fig. 15.

Some of this agreement needs to be explained in view of the two-dimensional nature of the model, which is applicable to slot injection and the three-dimensional nature of the flow out of a round hole in the experiments. As shown in Refs. 66 and 67, round jets in crossflows flatten out due to vortical kinematics as soon as one jet exit diameter along their length. The flattening process can legitimize the approximation that the curvature of the jet axis is more important than the circumferential one in determining the pressure jump across the jet.

In Figs. 14b and 16, the theoretical prediction is compared with instantaneous OH–PLIF images, which indicate the presence of the

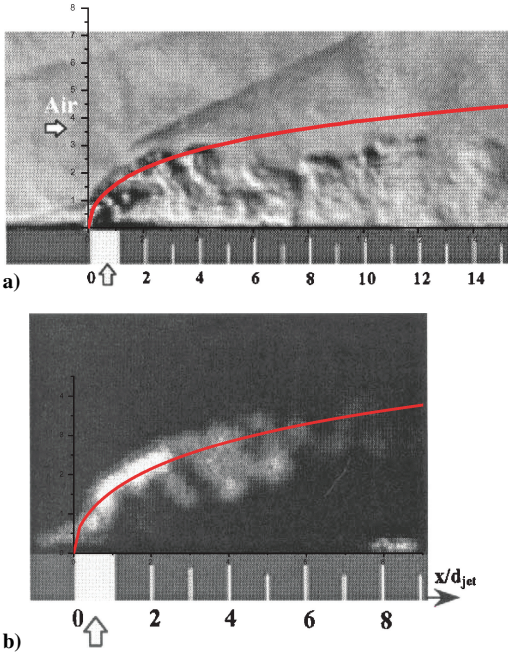

Fig. 14 Comparison of theoretical solution (20) (red line) with simultaneous a) schlieren and b) OH–PLIF images of hydrogen injection into supersonic crossflow[58]: $M = 3.46$, $T^* = 1300$ K, $p^* = 0.32$ psi, $U^*_\infty = 2420$ m/s, and the jet-to-freestream momentum flux ratio $\alpha = 1.4$.

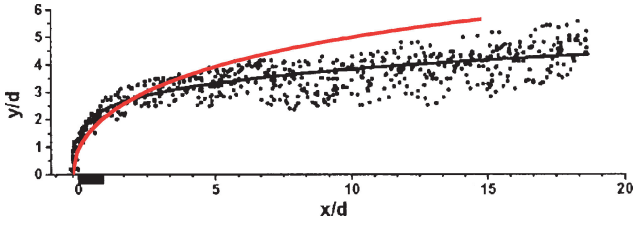

Fig. 15 Comparison of the theoretical solution (20) (red lines) with jet penetration measured from eight consecutive schlieren images of hydrogen injection into supersonic crossflow[52]: $M = 3.5$, $T^* = 1300$ K, $p^* = 0.32$ psi, $U^*_\infty = 2420$ m/s, and the jet-to-freestream momentum flux ratio $\alpha = 2$.

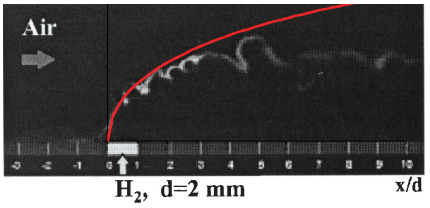

Fig. 16 Comparison of the theoretical solution (20) (red line) with simultaneous OH–PLIF image of hydrogen injection into supersonic crossflow[52]: $M = 3.5$, $T^* = 1300$ K, $p^* = 0.32$ psi, $U^*_\infty = 2420$ m/s, and the jet-to-freestream momentum flux ratio $\alpha = 2$.

OH radicals formed by the autoignition of jet hydrogen. The OH radicals are primarily produced in the hot separation region upstream of the jet exit (region 1 in Fig. 12) and directly behind the bow shock and are convected downstream with the shear-layer vortices. The OH-mole fraction decreases as the gases expand around the jet and the local mixture temperature falls.[52] In the near-field region, the solution (20) mimics the shape of a thin filament along the outer edge of the plume. Additional comparisons with experiment are given in Ref. 51. The theory breaks down and does not give the jet shock as a Mach line in the far-field region. This is because the jet interface is no longer close to the shock. In addition, the shock is attenuated and becomes weak. Accordingly, the thin-layer Newtonian assumptions are no longer applicable, and a linearized model involving the jet flow appearing as a Prandtl–Glauert supersonic sourcelike singularity in the far field may be applicable. Asymptotic modeling of this region and its matching with the near-field solution needs attention. Although the present model is not a formal asymptotic solution, it is a good starting point for such a systematic approximation scheme using the Newtonian distinguished limit. In spite of the aforementioned limitations, comparison of the theory in this paper and experiment reveals that it gives a good account of the physics important for fuel penetration estimation.

The scaling arising in terms of the jet-to-freestream momentum ratio parameter α (sometimes denoted as J in the literature) provides a means of collapsing normalized penetration data in units of jet exit width onto a universal curve shown by Srnivesan and Bowersox, as well as others, and arises naturally in our analysis. Indications are that the ideas of the present model with some modification apply to oblique injection. An important aspect of this work is that it can be used for a good first quantitative, nonempirical estimate of penetration of fuel into a hypersonic stream. The associated time and distance scales may be decisive in determining the fraction of fuel burned and other scramjet combustion metrics. This is being used in connection with our plasma jet ignition studies involving plasma chemistry modules and large-scale parallel computations to study the mixing processes in Ref. 68.

VI. Hypersonic Laminar Flow Control

A. Background

The ability to stabilize the hypersonic boundary layer and increase its laminar run is of critical importance in hypersonic vehicle design.[69] Early transition causes significant increases in heat transfer and skin friction. Higher heating requires a higher-performance thermal protection system (TPS), active cooling, or trajectory modification. This translates to higher cost and weight of hypersonic vehicles due to increased TPS weight. Moreover, with the low payload mass fraction, even a small savings in TPS weight can provide a significant payload increase.

Vehicle maintainability and operability are also affected by transition. Robust metallic TPS have temperature limits lower than ceramic TPS. Laminar flow control (LFC) can help to meet these more severe constraints. For a streamlined vehicle with large wetted area, viscous drag becomes important. It can be from 10% (fully laminar) to 30% (fully turbulent) of the overall drag.[70] For optimized hypersonic wave riders, viscous drag may represent up to 50% of

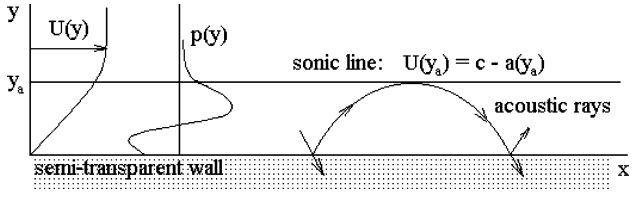

Fig. 17 Acoustic mode in supersonic boundary layer on semitransparent wall.

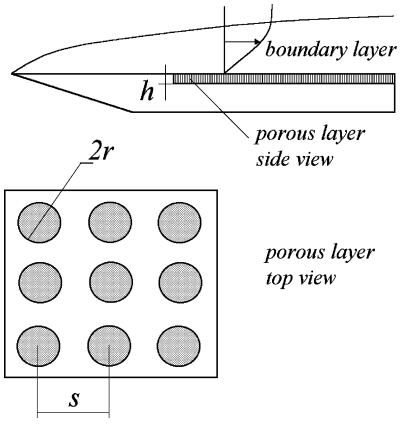

Fig. 18 Schematic of wall covered by porous layer.

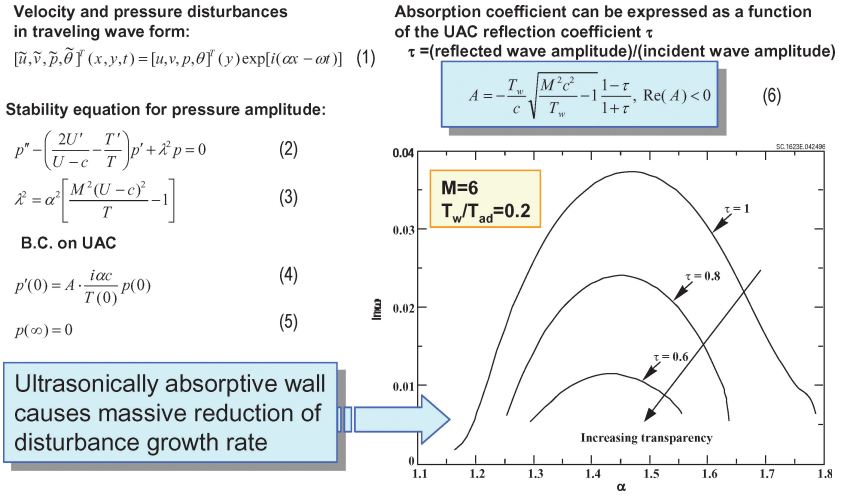

Fig. 19 Second mode instability control with UAC.

the total drag.[71] Vehicle aerodynamics is another area impacted by laminar–turbulent transition. Asymmetry of the transition locus can produce significant yawing moments. Aerodynamic control surfaces and reaction control systems are also affected due to the sensitivity of boundary-layer separation to the flow state (laminar or turbulent).

Because severe environmental conditions make it difficult to use active and reactive LFC concepts for hypersonic vehicles, passive LFC techniques are of great interest. As another example of a multiscale problem that is a challenge to conventional RANS approaches alone but accessible to a combination of theory, computation, and experiment, Malmuth et al.[72] developed a new passive method for stabilization of second and higher modes (Mack's acoustic modes). Without control and at hypersonic speeds, and although there are others such as crossflow, roughness, and Görtler types, the second mode instability provides a route to laminar–turbulent boundary-layer transition that is important to scramjet inlets and large acreage surfaces on hypersonic airbreathing cruise vehicles such as the X-43 Hyper-X. Although recent strategy has been to excite turbulence to promote scramjet ignition, it is well known that range and other performance metrics can benefit from laminarization of the inlets and other surfaces. The author believes that future vehicles will incorporate such improvements.

B. Control Concept

Malmuth et al.[72] exploited the fact that the hypersonic boundary layer behaves as an acoustic waveguide, schematically shown in Fig. 17. Therein, acoustic rays are reflected by the wall and turn around near the sonic line: $y=y_a$, and $U(y_a)=Re(c)-a(y_a)$, where c is disturbance phase speed, U is mean flow speed, and a is local sound speed. The second, third, and higher boundary-layer modes correspond to the waveguide normal modes. Fedorov et al.[73] assumed that the absorption of acoustic energy by an ultrasonically absorptive coating stabilizes these disturbances. This assumption was examined using stability theory for inviscid disturbances. It was found that an ultrasonically semitransparent wall provides substantial reduction of the second-mode growth rate.

To include viscous effects of the boundary layer, a second-mode stability analysis was performed for hypersonic boundary layers over walls covered by porous coatings with equally spaced blind microholes in Ref. 73.**[74] A schematic of the arrangement is shown in Fig. 18. Fourier decomposition was made in a linear stability characterization of the spatial and temporal parts of velocity, pressure, and temperature disturbances as shown in Eq. (1) of Fig. 19. This leads to the stability equation for the pressure amplitude (2) and (3), subject to Darcy-law-like boundary condition (4) on the ultrasonically absorbing wall (UAC). Absorption of the disturbance energy by porous layers was modeled using the theory of sound wave propagation in thin and long tubes to give the Darcy constant, admittance, or absorption coefficient A as shown in Eq. (6) of Fig. 19. The latter coefficient coupling the pressure disturbance with the vertical velocity disturbance on the porous surface is expressed as an explicit function of porosity characteristics. Stability calculations[73] showed that the dissipative absorption of disturbance energy by the porous coating provides massive reduction of the second mode growth rate in a wide range of disturbance frequencies and Reynolds numbers as indicated. This conclusion is consistent with the results by Malmuth et al.[72] obtained from their inviscid stability analysis. The most profound effect is observed on a cool wall that is typical for hypersonic vehicle TPS surfaces. A relatively thin porous coating (of thickness of about one-half of the laminar boundary-layer displacement thickness) provides a strong stabilization effect. Such porous coatings can be designed for passive laminar flow control in hypersonic vehicle surfaces. Note that the disturbance absorption should be produced at the initial phase of transition process where the unstable disturbance amplitude is about 0.01–0.1% of its level in transitional and turbulent boundary layers. In this phase, additional heating of the porous coating associated with partial absorption of the disturbance energy is negligibly small compared to the turbulent heating. Rasheed et al.[75] verified that the stabilization predicted by the theory actually delayed transition in experiments in the Graduate Aeronautical Laboratories, California Institute of Technology T-5 wind tunnel on a regular porosity coating. Later work by ITAM[76] further validated this delay and gave quantitative validation of the underlying theory in Ref. 73. Shown in panel a of Fig. 20 is a right circular cone that was tested in the tunnel. One-half of its surface consisted of the fine porous layer. The other half was an ordinary metal finish as shown in panel b. Panel c shows a dramatic increase in transition Reynolds number Re_{tr} at different enthalpy levels in the T-5 runs. In fact, with the porosity, no transition was noted on the model, and the laminar run was doubled. Panels d and e confirm this finding. New work in Ref. 76 shows excellent applicability of this concept for random porosity, providing a symbiotic relationship between natural TPS materials that are engineered to provide the UAC effect and a magnification of the aeroheating protection by laminarization. We intend to scale up this proof of concept to larger wind tunnels and ultimately deploy it on flight vehicles as schematically indicated for the X-43 configuration in Fig. 21.

VII. Other Examples

The foregoing four examples illustrate only a small subset of the tremendous benefit in using a triad of theory, computation, and experiment. In this connection, it is hoped that the value of the old pencil and pen analytical methods can be seen in the modern context described here. In addition to the examples given, we have used the triad on modeling counterflow and crossflow jets to simulate nose-tip plasma-jet aerospike drag reduction and plasma-jet enhanced

**One study of hypersonic boundary layers that provides useful information is Ref. 74.

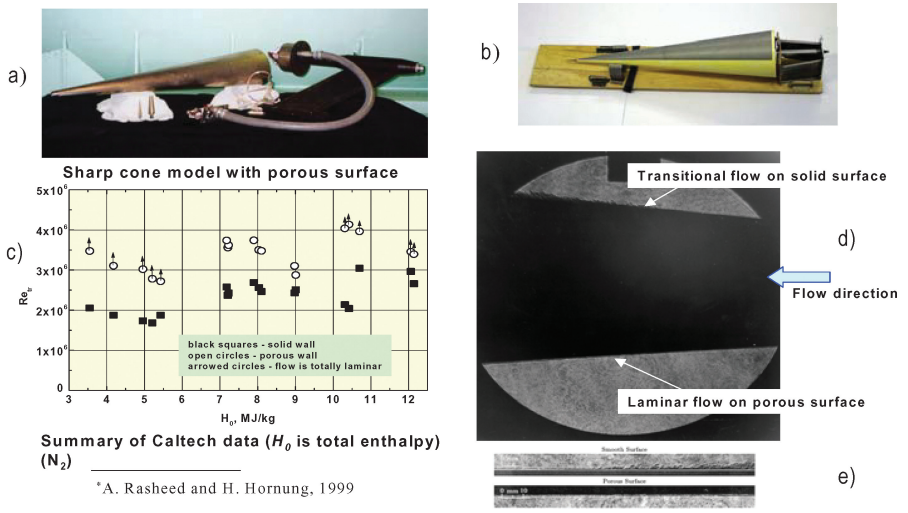

Fig. 20 California Institute of Technology and ITAM experiments showing that UAC substantially delays transition.

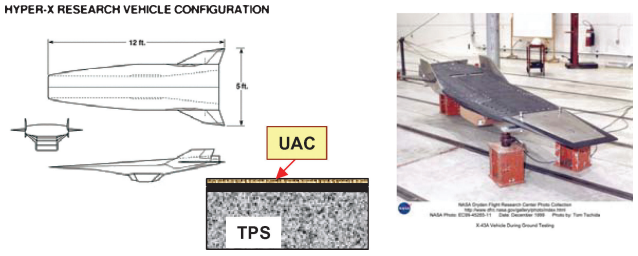

Fig. 21 Application of UAC concept for realistic airbreather.

scramjet ignition in Refs. 68 and 77. In addition, a gridless technique was developed to treat the problem of shock manipulation by magnetohydrodynamic (MHD) Lorentz forces in Ref. 78 that has been validated by large-scale CFD and experiments with the new MHD rig at ITAM. Additional use of the theoretical modeling showing the potential for forebody plasma streamers in reducing wave drag was described in Ref. 79. Modeling and experiment for use of plasma discharges for UAV and UCAV tailless and agile fighter nose-tip symmetry breaking control is given in Refs. 80 and 81.

VIII. Conclusions

In this paper, the state of theory with the present CFD emphasis in industry was reviewed. In addition to the many roles that were discussed, it is important that the educational system reinvigorate the concept that theoretical modeling is an indispensable tool to the engineer and scientist, in addition to the current emphasis on familiarity and use of legacy codes as well as the development of new ones. It still is a very important skill to know how to set up problems from first principles and make approximations for theoretical physics-based models, as well as to combine this capability with modern computational methods. In the author's opinion, suitable curricula need to be retained and student interest developed to foster these skills. These are very important even in the CFD environment when interpretation of the results is critical.

Acknowledgments

The author dedicates this paper to the memory of Professor Julian Cole, a mentor, close colleague, and friend of his for more than 40 years, who died in 1999. A portion of the research discussed was supported by Rockwell North American Aircraft. In addition, the author gratefully acknowledges the invaluable continuing support of Arje Nachman of the U.S. Air Force Office of Scientific Research, U.S. Air Force Materials Command, under Grant 88-0037 and Contracts F49620-92-C-0006, F49620-96-C-0004, F49620-99-C-0005, F49620-02-C-0024, and FA9550-05-C-0030 and Julian Tishkoff of the U.S. Air Force Office of Scientific Research, U.S. Air Force Materials Command under contracts F499620-01-C-0037 and FA9550-04-C-0028. The author is indebted to Elwood Bonner (deceased), formerly of North American Aviation, Inc., for valuable discussions and support, as well as constructive comments by Katerina Kaouri, Oxford Centre for Industrial and Applied Mathematics Mathematical Institute, Oxford University; Oleg Ryzhov, University of California, Davis, Zvi Rusak, Rensselaer Polytechnic Institute; Alexander Fedorov and Valdimir Shalaev, Moscow Institute of Physics and Technology; Anatoly Maslov of the Institute of the Theoretical and Applied Mechanics in Novosibirsk, Russia; Vladimir Bytchkov, Moscow State University; and Victor Soloviev of Moscow Institute of Technology. Additional valuable collaboration with Dave Williams, IIT; Hans Hornung and Tim Colonius of the California Institute of Technology; and Don Picetti, Sergio Carrion, Bill Bower, Val Kibens, Phil Smereczniak, and Joe Silkey of The Boeing Company was helpful in preparing this paper. Editorial comments by T. F. Zien are also appreciated. The U.S. government is authorized to reproduce and distribute reprints for government purposes, notwithstanding any copyright notation thereon. The views and conclusions herein are those of the authors and should not be interpreted as necessarily representing the official policies or endorsements, either expressed, or implied of the Air Force Office of Scientific Research or the U.S. government.

References

[1]Cosner, R., "Assessment of Vehicle Performance Predictions Using CFD," AIAA Paper 2000-0384, 2000.

[2]Lee-Rausch, E. M., Buning, P. G., Mavriplis, D., Morrison, J. H., Park, M. A., Rivers, S. M., and Rumsey, C. L., "CFD Sensitivity Analysis of a Drag Prediction Workshop Wing/Body Transport Configuration," AIAA Paper 2003-3400, 2003.

[3]Malmuth, N., et al., "Management of Transitional Separation for Flow Control of Military Flight Vehicles," NATO Research and Technology Organization Air Vehicle Technology Specialist Meeting, Paper AVT-111, Oct. 2004.

[4]Bluman, G. W., and Cole, J. D., *Similarity Methods for Differential Equations*, Vol. 13, Applied Mathematics Sciences, Springer-Verlag, 1974.

[5]Kevorkian, J., and Cole, J., *Perturbation Methods in Applied Mathematics*, Springer-Verlag, New York, 1981.

[6]Sears, W. (ed.), *General Theory of High Speed Aerodynamics, Vol. VI, High Speed Aerodynamics and Jet Propulsion*, Princeton Univ. Press, Princeton, NJ, 1954.

[7]Cole, J., and Cook, L., *Transonic Aerodynamics*, North-Holland, New York, 1986.

[8]Guderley, K., *Theory of Transonic Flow*, Addison Wesley, Longman, 1962.

[9]Cole, J. D., "Newtonian Flow Theory for Slender Bodies," *Journal of Aerospace Sciences*, Vol. 24, 1957, pp. 448–455.

[10]Jones, R. T., "Properties of Low-Aspect-Ratio Pointed Wings at Speeds Below and Above the Speed of Sound," NACA Rept. 835, 1946.

[11]Diesperov, V., Lifshitz, Y., and Ryzhov, O., *Archives of Mechanics*, Vol. 26, No. 3, 1974, pp. 511–521.
[12]Diesperov, V., Lifshitz, Y., and Ryzhov, O., *Symposium Transsonicum, II*, Springer, 1976.
[13]Lagerstrom, P., "Laminar Flow Theory," *Theory of Laminar Flows, High Speed Aerodynamics and Jet Propulsion, Vol. IV*, edited by F. Moore, Princeton Univ. Press, Princeton, NJ, 1964, Sec. B, pp. 20–150.
[14]Lagerstrom, P., *Matched Asymptotic Expansions, Ideas and Techniques*, Applied Mathematical Sciences 76, Springer-Verlag, New York, 1988.
[15]Ryzhov, O., AIAA Paper 2005-4803, 2005.
[16]Rusak, Z., *Journal of Fluid Mechanics*, Vol. 248, 1993, pp. 1–26.
[17]Rusak, Z., *European Journal of Applied Mechanics*, Vol. 5, 1994, pp. 283–311.
[18]Lax, P., "Weak Solutions of Nonlinear Hyperbolic Equations and Their Numerical Computation," *Communications in Pure and Applied Mathematics*, Vol. 7, 1954, pp. 159–193.
[19]Magnus, R., and Yoshihara, H., "Inviscid Transonic Flow over Airfoils," *AIAA Journal*, Vol. 8, No. 12, 1970, pp. 2157–2162.
[20]Murman, E., and Cole, J., "Calculation of Plane Transonic Flows," *AIAA Journal*, Vol. 9, 1971, pp. 114–121.
[21]Spreiter, J., "The Local Linearization Method in Transonic Flow Theory," *Symposium Transsonicum*, Springer-Verlag, Berlin, 1964, pp. 152–183.
[22]Edney, B., "Anomalous Heat Transfer and Pressure Distributions on Blunt Bodies at Hypersonic Speeds in the Presence of an Impinging Shock," FFA, Rept. 115, Stockholm, 1968.
[23]Oswatitisch, K., and Keune, F., "Ein Äquivalenzsatz für Nichtangestellet Flügel Kleiner Spannweite in Schallnaher Strömung," *S. Flugwiss*, Vol. 3, No. 2, 1955, pp. 29–46.
[24]Cole, J., and Malmuth, N., "Wave Drag of Transonic Airplanes," *Proceedings of the Royal Society of London, Series A: Mathematical and Physical Sciences*, Vol. 461, No. 2054, 2005, pp. 541–560.
[25]Cheng, H. K., and Hafez, M. M., "Equivalence Rule and Transonic Flow Theory Involving Lift," *AIAA Journal*, Vol. 11, No. 8, 1973, pp. 1210–1212.
[26]Barnwell, R. W., "Analysis of Transonic Flow About Lifting Wing-Body Configurations," NASA TR R-440, June 1975.
[27]Cramer, M. S., "Lifting Three-Dimensional Wings in Transonic Flow," *Journal of Fluid Mechanics*, Vol. 95, 1979, pp. 223–240.
[28]Cramer, M. S., "A Note on 'Lifting Three-Dimensional Wings in Transonic Flow,'" *Journal of Fluid Mechanics*, Vol. 109, 1981, pp. 257, 258.
[29]Milne Thomson, L., *Theoretical Hydrodynamics*, 3rd ed., Macmillan, New York, 1955.
[30]Schindel, L. H., "Store Separation," Rept. AG-202, AGARD, June 1975.
[31]Goodwin, F. K., Dillenius, M. F. E., and Nielsen, J. N., "Prediction of Six-Degree-of-Freedom Store Separation Trajectories at Speeds Up to the Critical Speed. V.1. Theoretical Methods and Comparison with Experiment," U.S. Air Force Flight Dynamics Lab., Rept. AFFDL-TR-72-83, 1972.
[32]Wood, M. E., "Application of Experimental Techniques to Store Release Problems," Proceedings of NEAR Conf. on Missile Aerodynamics, 1988.
[33]Prewitt, N. C., Belk, D. M., and Maple, R. C., "Multiple Body Trajectory Calculations Using the Beggar Code," *Journal of Aircraft*, Vol. 36, No. 5, 1999, pp. 802–808.
[34]Lijewski, L., and Suhs, N. E., "Time-Accurate Computational Fluid Dynamics to Transonic Store Separation Trajectory Prediction, *Journal of Aircraft*, Vol. 31, No. 4, 1994, pp. 886–891.
[35]Sickles, W., Denny, A., and Nichols, R., "Time-Accurate CFD Predictions of the JDAM Separation from an F-18C Aircraft," AIAA 00-0796, Jan. 2000.
[36]Rizk, M., Ellison, S., and Prewitt, N., "Beggar—A Store Separation Predictive Tool," AIAA 2002-3190, June 2002.
[37]Murphy, K., Buning, P., Pamadi, B., Scallion, W., and Jones, K., "Overview of Transonic to Hypersonic Stage Separation Tool Development to Multi-Stage-to-Orbit Concepts," AIAA 2004-2595, June 2004.
[38]Murman, S., Aftosmis, M., and Berger, M., "Simulations of 6-DOF Motion with a Cartesian Method," AIAA Paper 2003-1246, Jan. 2003.
[39]Murman, S., Aftosmis, M., and Berger, M., "Implicit Approaches for Moving Boundaries in a 3-D Cartesian Method," AIAA Paper 2003-1119, Jan. 2003.
[40]Liever, P., and Habchi, S., "Separation Analysis of Launch Vehicle Crew Escape Systems, AIAA Paper 2004-4726, 2004.
[41]Aradag, S., and Knight, D., "Simulation of Supersonic Cavity Flow Using 3D RANS Equations," AIAA Paper 2004-4966, Aug. 2004.
[42]Rizzetta, D. P., and Visbal, M. R., "Large-Eddy Simulation of Supersonic Cavity Flowfields Including Flow Control," *AIAA Journal*, Vol. 41, No. 8, 2003, pp. 1452–1462.
[43]Colonius, T., Basu, A., and Rowley, C., "Numerical Investigation of the Flow past a Cavity," AIAA Paper 99-1912, 1999.
[44]Bjorge, S., Reeder, M., Subramanian, C., and Crafton, J., "Flow Around an Object Projected from a Cavity into a Freestream," AIAA Paper 2004-1253, 2004.
[45]Bower, W., Kibens, V., Cary, A., Alvi, F., Annaswamy, A., and Malmuth, N., "High-Frequency Active Control for High-Speed Weapon Release (HIFEX)," AIAA Paper 2004-2513, June 2004.
[46]Shalaev, V., Fedorov, A., and Malmuth, N., "Dynamics of Slender Bodies Separating from Rectangular Cavities," *AIAA Journal*, Vol. 40, No. 3, 2002, pp. 517–525.
[47]Shalaev, V., Malmuth, N., and Fedorov, A., "Analytical Modeling of Transonic Store Separation from a Cavity," AIAA Paper 2003-0004, Jan. 2003.
[48]Malmuth, N., and Shalaev, V., "Theoretical Modeling of Slender Bodies Interaction in Supersonic Flows," AIAA Paper 2004-1127, Jan. 2004.
[49]Quirk, J., "Amrita—A Computational Facility (for CFD modeling)," *VKI 29th CFD Lecture Series*, von Kármán Inst., 1988.
[50]Malmuth, N., Hites, M., and Williams, D., "Photographic Investigation of the Dynamics of an Ogive Model near a Cavity at Subsonic Mach Numbers," Final Rept., Fluid Dynamics Research Center, Illinois Inst. of Technology, Jan. 1998.
[51]Malmuth, N., and Fedorov, A., "Thin Shock Layer Model for a Jet in a Hypersonic Cross Flow," AIAA Paper 2005-0893, 2005.
[52]Ben-Yakar, A., and Hanson, R. K., "Supersonic Combustion of Cross-Flow Jets and the Influence of Cavity Flame-Holders," AIAA Paper 99-0484, 1999.
[53]Krasnov, N. F., Koshevoy, V. N., and Kalugin, V. T., *Aerodynamics of Separated Flows*, Vysshaya Shkola, Moscow, 1988 (in Russian).
[54]Ben-Yakar, A., and Hanson, R.K., "Experimental Investigation of Flame-Holding Capability of Hydrogen Transverse Jet in Supersonic Cross-Flow," *27th Symposium on Combustion*, Combustion Inst., 1998, pp. 2173–2180.
[55]McDaniel, J. C., and Graves, J., "Laser Induced Fluorescence Visualization of Transverse Gaseous Injection in a Nonreacting Supersonic Combustor," *Journal of Propulsion and Power*, Vol. 4, No. 6, 1988, pp. 591–597.
[56]Gruber, M. R., Nejad, A. S., Chen, T. H., and Dutton, J. C., "Mixing and Penetration Studies of Sonic Jets in a Mach 2 Freestream," *Journal of Propulsion and Power*, Vol. 11, No. 2, 1995, pp. 315–323.
[57]Rothstein, A. D., and Wantuck, P. J., "A Study of the Normal Injection of Hydrogen into a Heated Supersonic Flow Using Planar Laser-Induced Fluorescence," AIAA Paper 92-3423, 1992.
[58]Ben-Yakar, A., Kamel, M. R., Morris, C. I., and Hanson, R. K., "Experimental Investigation of H_2 Transverse Jet Combustion in Hypervelocity Flows," AIAA Paper 97-3019, 1997.
[59]Srnivesan, R., and Bowersox, R., "Detached Eddy Simulation of Gaseous into a Mach 5.0 Freestream," AIAA Paper 2005-0893, Jan. 2005.
[60]Liepmann, H., and Roshko, A., *Elements of Gasydnamics*, Wiley, New York, 1957.
[61]Chernyi, G. G., *Introduction to Hypersonic Flow*, translated by R. F. Probstein, Academic Press, New York, 1961, pp. 209, 215.
[62]Sedov, L. I., *Similarity and Dimensional Methods in Mechanics*, English translation, edited by M. Holt, Academic Press, New York, 1959.
[63]Taylor, G. I., "The Formation of Blast Wave by a Very Intense Explosion," *Proceedings of the Royal Society of London, Series A: Mathematical and Physical Sciences*, Vol. 201, 1950, pp. 159–186.
[64]Hayes, W., and Probstein, R., *Hypersonic Flow Theory*, Academic Press, New York, 1959.
[65]Cheng, H. K., "Inviscid Leading Edge Effect in Hypersonic Flow," *Journal of the Aeronautical Sciences*, Vol. 23, 1956, pp. 898–900.
[66]Abramovich, G., *The Theory of Turbulent Jets*, English translation by Scripta Technica, MIT Press, 1963, pp. 541–556.
[67]Shandorov, G., "Flow from a Channel into Stationary and Moving Media," *Zh. Tekn. Fiz*, Vol. 37, No. 1, 1957.
[68]Ardelyan, N., Bytchkov, V., Kosmachevskii, K., Malmuth, N., and Timofeev, I., "Plasma Generators with Divergent Channel for Aerodynamic Applications," AIAA Paper 2004-0179, Jan. 2004.
[69]Malik, M. R., Zang, T. A., and Bushnell, D. M., "Boundary Layer Transition in Hypersonic Flows," AIAA Paper 90-5232, 1990.
[70]Reed, H. L., Kimmel, R., Schneider, S., and Arnal, D., "Drag Prediction and Transition in Hypersonic Flow," AIAA Paper 97-1818, June 1997.
[71]Bowcutt, K. G., Anderson, J. D., and Capriotti, D., "Viscous Optimized Hypersonic Waveriders," AIAA Paper 87-0272, 1987.
[72]Malmuth, N., Fedorov, A., Shalaev, V., Cole, J., and Khokhlov, A., "Problems in High Speed Flow Prediction Relevant to Control," AIAA Paper 98-2995, June 1998.
[73]Fedorov, A., Malmuth, N., Rasheed, A., and Hornung, H., "Stabilization of Hypersonic Boundary Layers by Porous Coatings," *AIAA Journal*, Vol. 39, No. 4, 2002, pp. 605–610.
[74]Brown, S., Khorami, A. F., Neish, A., and Smith, F. T., "On Hypersonic Boundary-Layer Interactions and Transitions," *Philosophical Transactions of the Royal Society of London*, Vol. 335A, 1991, pp. 139–152.
[75]Rasheed, A., Hornung, H., Fedorov, A., and Malmuth, N., "Experiments on Passive Hypersonic Boundary-Layer Control Using a Porous Surface," *AIAA Journal*, Vol. 40, No. 3, 2002, pp. 481–489.

[76]Fedorov, A., Shiplyuk, A., Maslov, A., Burov, E., and Malmuth, N., "Stabilization of a Hypersonic Boundary Layer Using an Ultrasonically Absorptive Coating," *Journal of Fluid Mechanics*, Vol. 479, 2003, pp. 99–124.

[77]Fomin, V., Maslov, A., Malmuth, N., Fomichev, V., Shashkin, A., Korotaeva, T., Shipyuk, A., and Pozdnyakov, G., "Influence of Counterflow Plasma Jet on Supersonic Blunt-Body Pressures," *AIAA Journal*, Vol. 40, No. 6, 2002, pp. 1170–1177.

[78]Malmuth, N., Krivstov, V., and Soloviev, V., "Quick Gridless Estimation of MHD Effects on Hypersonic Inlet Ramp Shocks," AIAA Paper 2004-0862, 2004.

[79]Soloviev, V., Kristov, K., Konchakov, A., and Malmuth, N., "Drag Reduction by Plasma Filaments Over Supersonic Forebodies," *AIAA Journal*, Vol. 41, No. 12, 2003, pp. 2403–2409.

[80]Maslov, A., Zanin, B., Sidorenko, A., Fomichev, V., Postnikov, B., and Malmuth, N., "Plasma Control of Separated Flow Asymmetry on a Cone at High Angle of Attack," AIAA Paper 2004-0843, Jan. 2004.

[81]Shalaev, V., Fedorov, A., Malmuth, N., and Shalaev, I., "Mechanism of Forebody Nose Vortex Symmetry Breaking Relevant Plasma Flow Control," Jan. 2004.

E. Oran
Editor-in-Chief

Color reproductions courtesy of Rockwell Scientific Company.